nature portfolio

Peer Review File

Secondary nucleation guided noncovalent synthesis of dendritic homochiral superstructures via growth on and from surface

Corresponding Author: Dr Venkata Rao Kotagiri

This file contains all reviewer reports in order by version, followed by all author rebuttals in order by version.

Attachments originally included by the reviewers as part of their assessment can be found at the end of this file.

Version 0:

Reviewer comments:

Reviewer #1

(Remarks to the Author)
In this manuscript, Rao et al. report the synthesis of dendritic homochiral superstructures through the supramolecular polymerisation of NIR triimide dyes. The formation of these superstructures initiates with a primary nucleation step, followed by secondary nucleation events occurring both ‘on the surface’ and ‘from the surface’ of the polymer.

The resulting superstructures, which can reach up to 0.4 mm^2 in size, consist of a central superhelix from which numerous branched smaller helices extend, all of which are homochiral and dependent on the chirality of the monomeric unit. These superstructures were characterized using electronic microscopy and standard spectroscopic techniques. The decrease in absorbance at 650 nm allowed the authors to monitor the kinetics of superstructure formation and to elucidate the mechanism through the various nucleation steps. These chiral superstructures exhibited remarkably high chiroptical responses.

The superstructures presented by the authors are both a rare and elegant display of supramolecular chemistry. The microscopy images unambiguously demonstrate the formation of dendritic superstructures composed of homochiral helices, which are directly emerging from the chirality of the building blocks.

I like the concept of the paper, yet I am a hesitant to accept it immediately. This hesitation stems (amongst other things) from the fact that kinetics are dominant in this polymerization which could make reproduction difficult. No thermodynamic experiments were performed in the whole manuscript to demonstrate otherwise. I wonder if the same supramolecular polymers could form after heating-cooling pretreatment.

Thus, I insist that the full sample preparation is included in the article. Furthermore, I would like to see that multiple concentrations of S-G are used for the UV-VIS/CD experiments to determine if a certain threshold needs to be reached for high aggregation to occur. I must also express some concern that the investigation of only four different concentrations, with limited variation between them (20–35 μM), might be insufficient to draw definitive conclusions regarding the nucleation mechanism.In the model cited by the authors for secondary nucleation polymerization (Nat. Prot. 11, 252- 272 (2016)), twice as many data points were used to arrive at similar conclusions. It would also be beneficial to study the influence of temperature on the formation of the superstructures.

It is exciting to see the application of amylofit in supramolecular polymers. However, the procedures need to be performed very carefully. The discussion and conclusion based on amylofit are not convincing to me as the following questions: 1) a very important factor that can significantly influence the kinetical experiment is to exclude the existence of any small aggregates as it can remarkably change the observed kinetics. The samples prepared in this work were by diluting a 1 mM stock solution of S/R-G in CHCl3. Dilution is not a way to remove kinetic trapped aggregates, for this reason, it is very important to make sure there are no aggregates existing in 1 mM CHCl3 solution. Variable concentration experiments in CHCl3 (UVvis or HNMR) should be conducted to exclude the possibility. 2) A clear biphasic behavior was observed in the kinetic profiles of aggregation at the concentrations of 30 uM and 35 uM. Those often come from poor control of initial

conditions which further increase my first concern that small aggregates existed in the stock solution. One also should notice that these data are unsuitable for the fitting analysis. 3) I think that The support for the conclusion that “The absence of curvature in the linear fit suggests that it should align well with the secondary nucleation mechanism” is weak. First of all, the linear fitting in my opinion is very poor (let alone the high concentration data are not reliable). Secondly, a more intuitive conclusion based on this experiment is that it is negative curvature, indicating that competition exists. Thirdly (and again), at least 8-10 sets of data need to be obtained to get a reliable and accurate scaling exponent value.

In conclusion, this is fantastic work that will benefit clearly from some more experimental work. I recommend this manuscript for publication in Nature Communications following the major revisions suggested above.

Additional comments

- The FE-SEM images presented in this manuscript are spectacular. However, to further demonstrate the concept of “dendritic homochiral superstructures”, AFM is required to investigate the helicity of branch fibers.
- Can the aggregates be ‘reset’ to the monomeric state via heating (VT curves) or sonication?
- Did the authors check if in-solution IR be used to follow the change in functional groups and subsequently determine the driving force of assembly?
- Figure 1 is misleading since it displays that aggregation only starts on a surface while Figure 2C clearly shows that aggregation is also happening in solution.
- Figure 2: 4 different periods are used in the figures which makes it more difficult to compare that it should be. Also, why was it chosen to have for 2B only a window of 25 minutes? Was the CD signal decreasing after 25 minutes due to it potentially crashing out of solution?
- Were Linear dichroism (LD) measurements considered to determine the starting point of aggregation? 1D polymer cannot display an LD signal while aggregates will. LD should also be performed to know if LD contributes to the CD signals obtained in the manuscript. On the other hand, it will be interesting to see if preferential oriented supramolecular polymers were formed in solution after 25 mins.
- The IR of the enantiomers differs quite considerably which seems odd.
- Figure S12: what is the difference between A and B?

Reviewer #2

(Remarks to the Author)
In this manuscript, the authors report the non-covalent synthesis of dendritic purely chiral superstructures by a secondary nucleation extension process using NIR triimide dyes as building blocks. The analysis of the kinetics and time evolution of the morphology shows that the formation of dendritic homochiral superstructures proceeds via growth on the surface and growth from the surface of the crystal species. The combination of these two processes leads to the formation of elegant homochiral superstructures with dimensions of about 0.4 mm2, with a superhelix at the center and helical fibers as branches. Moreover, these dendritic homochiral superstructures exhibit significantly high chiral optical photoresponse with gfactor sizes reaching values up to 0.55-0.6. This work is original and well-organized, and I recommend to accept this manuscript for publication in Nature Communications. Some suggestions and concerns are listed as follows.
(1) Since the self-assembly proceed in two stages: growth on the surface and growth from the surface. Is it possible to discerned the two stages from the absorption and CD spectra in Figure 2a and 2b?
(2) From Figure 2c, the sample seems precipitated in 15 minutes during the self-assembly (30 M, 15% CHCl3 in IPA). So, are the UV-vis and CD spectra recorded under the same conditions (30 M, 15% CHCl3 in IPA, 0-48 minutes) reliable?
(3) Since the monomers are pure chirality, the helicity of the self-assembled fibers is suggested to discuss? For example, how about the excess of one-handed helix of the supramolecular nanofibers? Or they self-assembled into a single left- or right-handed supramolecular helices? This is important to confirm the self-assemblies are real DHS.
(4) Can the helical nanofibers directly emit CPL light?
(5) For comparison, the CD spectra of the self-assemblies of R-G are suggested to provide in Figure 2b in the main.
(6) For the UV-Vis absorption spectra (Figure 2a), the authors tested for 48 min while the CD spectra (Figure 2b) was only 25 minutes, could the authors please describe the reason for this?
(7) How about the self-assembly of S- and R-G in different molar ratios?
(8) Some important papers related to this paper closely are encouraged to cite, such as Chem. Sci. 2024, 15, 2946–2953. Acc. Chem. Res. 2023, 56, 2954-2967. Angew. Chem. Int. Ed. 2022, 61, e202207028. Angew. Chem., Int. Ed. 2020, 59, 16675–16682.

Reviewer #3

(Remarks to the Author)
[Note from editor: please see attachment]

Version 1:

Reviewer comments:

Reviewer #1

(Remarks to the Author)
All of my comments and concerns have been well and thoroughly addressed in this
new version. I congratulate the authors on this beautiful work and thank them for investing the time to substantially improve the previous version! I would like to recommend to accept this paper as is.

Reviewer #2

(Remarks to the Author)
The manuscript has been properly revised and can be accepted for publication.

Reviewer #3

(Remarks to the Author)
The discovery is intriguing. Following the initial review process, the authors have conducted additional experiments, including the synthesis of achiral model compounds and relevant calculations. Overall, the quality of the paper has improved by addressing the feedback from the three reviewers. However, some formatting issues still need to be addressed, such as maintaining consistency in time units (e.g., 'sec' vs. 'seconds'), correcting grammatical errors, and ensuring uniformity in the range and height of the ^1H NMR spectra.

NCOMMS-24-46135-T

Point-to-Point responses to the reviewer's comments

We appreciate all the reviewers for their time and effort in going through our manuscript and providing valuable comments. The comments were very useful and significantly improved the quality and understanding of our results. We have revised the manuscript by addressing all the comments of the reviewers with additional experiments and theoretical calculations. We hope that the revised manuscript is now suitable for publication in *Nature Communications*.

Changes made to the article based on reviewer comments are shaded with yellow colour.

Reviewer 1

1. In this manuscript, Rao et al. report the synthesis of dendritic homochiral superstructures through the supramolecular polymerization of NIR triimide dyes. The formation of these superstructures initiates with a primary nucleation step, followed by secondary nucleation events occurring both 'on the surface' and 'from the surface' of the polymer. The resulting superstructures, which can reach up to 0.4 mm^2 in size, consist of a central superhelix from which numerous branched smaller helices extend, all of which are homochiral and dependent on the chirality of the monomeric unit. These superstructures were characterized using electronic microscopy and standard spectroscopic techniques. The decrease in absorbance at 650 nm allowed the authors to monitor the kinetics of superstructure formation and to elucidate the mechanism through the various nucleation steps. These chiral superstructures exhibited remarkably high chiroptical responses.

   The superstructures presented by the authors are both a rare and elegant display of supramolecular chemistry. The microscopy images unambiguously demonstrate the formation of dendritic superstructures composed of homochiral helices, which are directly emerging from the chirality of the building blocks.

   Ans. We thank the reviewer for elegantly summarising our work and positive feedback.

2. I like the concept of the paper, yet I am a hesitant to accept it immediately. This hesitation stems (amongst other things) from the fact that kinetics are dominant in this polymerization which could make reproduction difficult. No thermodynamic experiments were performed in the whole manuscript to demonstrate otherwise. I wonder if the same supramolecular polymers could form after heating-cooling pretreatment.

   Ans. We thank the reviewer for the positive comments on our work and important suggestions regarding thermodynamic data. In fact, we have explored temperature-dependent experiments to obtain the thermodynamic parameters. However, in the given solvent conditions (85% IPA in $CHCl_3$), the assemblies could not be completely depolymerized into monomers. For example, a 30 μM as prepared solution (85% IPA in $CHCl_3$) was heated to 65 °C. The spectrum obtained at 65 °C does not resemble the monomeric spectrum of ***S*-G** in $CHCl_3$, but has increased absorbance, indicating that it does not go back to fully monomeric state upon heating (Supplementary Figure 29a). The morphology obtained of the heated solution is small helical fibers (Supplementary Figure 29d). We cannot go beyond 65 °C due to evaporation of $CHCl_3$. To overcome this issue, we heated a 15 μM solution of ***S*-G** to 65 °C. In this case also, the absorption spectrum does not resemble the monomeric spectrum of

$CHCl_3$ (Supplementary Figure 29b). So, it is difficult to monitor the thermodynamics. Further, we cooled the 30 µM hot solution from 65 °C to 25 °C at a cooling rate of 1K/min. The spectrum obtained after reaching 25 °C, is same as what was obtained for as prepared solution. This solution, upon keeping at 25 °C for ~48 minutes, formed DHS structure as confirmed by FE-SEM images (Supplementary Figure 29e). Thus, we can conclude that though upon heating, the solution does not go back to the monomeric state, upon heating-cooling pretreatment, DHS are formed.

This data is included in the revised manuscript as Supplementary Figure 29a,b,d,e

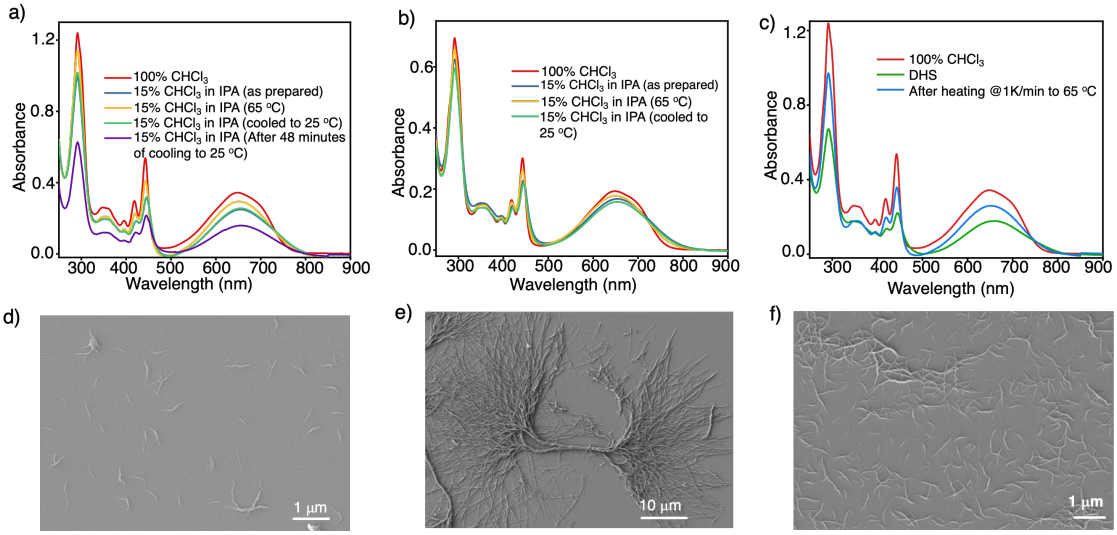

Supplementary Figure 29. (a) Effect of temperature on the absorption spectra of ***S*-G**. Heating of an as prepared solution of 30 µM in 15% $CHCl_3$ in IPA at 65 °C and its comparison with monomer (100% $CHCl_3$). After cooling back to 25 °C, the spectrum is similar to as prepared solution (15% $CHCl_3$ in IPA). (b) Effect of temperature on the absorption spectra of 15 µM solution of ***S*-G** in 15% $CHCl_3$ in IPA at 65 °C and its comparison with monomer (100% $CHCl_3$). (c) Absorption spectra of DHS of ***S*-G** and its comparison with 100 % $CHCl_3$. Upon heating, this solution does not go back to the monomeric state. FE-SEM images of a 30 µM solution of ***S*-G** in 15% $CHCl_3$ in IPA (d) heated up to 65 °C and spin-coated on silicon wafer and (e) DHS formed after it was cooled back to 25 °C and waited for 48 minutes and spin-coated on silicon wafer. (f) FE-SEM image obtained by spin-coating the hot solution of DHS solution, which was heated to 65 °C.

The Following sentences were added to the main text on page 11, top paragraph.

"To understand whether ***S*-G** in 15% $CHCl_3$ in IPA can be completely depolymerized into monomers, a freshly prepared solution of 30 µM solution of ***S*-G** in 15% $CHCl_3$ in IPA was heated to 65 °C. Although absorbance is increased compared to that of at 25 °C, but could not reach like monomers in pure $CHCl_3$, indicating incomplete depolymerized into monomers even at 65 °C (Supplementary Figure 29a,d). We could not go beyond 65 °C due to the evaporation of $CHCl_3$. When this solution is cooled back to 25 °C, the absorption spectrum obtained is similar to the freshly prepared solution at 25 °C. After allowing it at 25 °C for 48 minutes, the formation of DHS was observed, as evidenced by the FE-SEM images (Supplementary Figure 29a,e). We have also tried the 15 µM solution of ***S*-G** in 15% $CHCl_3$ in IPA, but complete depolymerization into monomers is not observed at 65 °C (Supplementary Figure 29b). Similarly, after the formation of DHS (30 µM), the solution was heated at 65 °C, but complete depolymerization was not observed (Supplementary Figure 29c). When this hot solution was spin-coated on a silicon wafer and visualized using FE-SEM, short helical fibres were observed (Supplementary Figure 29f). This indicates that in 15% $CHCl_3$ in IPA at 65 °C, DHS can be dissociated into short helical fibres but not completely into monomers."

3. Thus, I insist that the full sample preparation is included in the article.

Ans. We thank the reviewer for this comment. The following full revised sample preparation has been included in the revised manuscript in the methods section.

"**DHS preparation:** 2 mg of ***S*-G/*R*-G** was measured and transferred into a vial and 2.6 ml of $CHCl_3$ was added to it to obtain a concentration of 1 mM, which is the stock solution. Concentration dependent experiments of ***S*-G** by varying the concentration from 100 μM to 300 μM performed in $CHCl_3$ using UV-Vis absorption spectroscopy revealed a linear relation (Supplementary Figure 35), indicating the absence of any preexisting aggregates of ***S*-G/*R*-G** in $CHCl_3$ solution before the addition of IPA. From the 1 mM $CHCl_3$ stock solution, 90 μL was transferred into a vial and 350 μL of $CHCl_3$ (good solvent) was added. To this, a further 2550 μL of IPA (poor solvent) was added and mixed well to make the whole volume 3 mL containing 30 μM of ***S*-G/*R*-G** in 15% of $CHCl_3$ in IPA. These solutions were used for UV-Vis spectroscopy and CD measurements as such."

4. Furthermore, I would like to see that multiple concentrations of ***S*-G** are used for the UV-VIS/CD experiments to determine if a certain threshold needs to be reached for high aggregation to occur.

Ans. We thank the reviewer for this suggestion. We have performed experiments to identify threshold for higher aggregation to occur. By lowering concentration to 15 μM and 10 μM, we have monitored time-dependent absorption spectra of ***S*-G** in 15% $CHCl_3$ in IPA. The 15 μM solution completed self-assembly within 7000 seconds (Figure 4c) but the lower concentration of 10 μM does not show any further change in the absorption spectrum even after 10,800 seconds (3 hours) (Supplementary Figure 25). Thus, we conclude that the threshold for higher aggregates to form is 15 μM.

The time-dependent absorption spectra of ***S*-G** at 10 μM is added Supplementary Figure 25 in the revised manuscript.

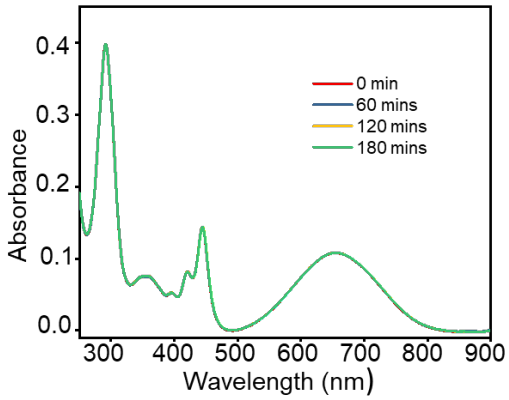

Supplementary Figure 25. Absorption spectra of a 10 μM solution of ***S*-G** in 15% $CHCl_3$ in IPA, monitored over a period of 180 minutes (3 hours).

The following sentences are included in the revised manuscript in page 7, bottom paragraph.

"We found that 15 μM is the threshold concentration because, at 10 μM, no significant changes in the absorption spectra were observed even for 3 hours at 25 °C (Supplementary Figure 25)."

5. I must also express some concern that the investigation of only four different concentrations, with limited variation between them (20–35 μM), might be insufficient to draw definitive conclusions regarding the nucleation mechanism. In the model cited by the authors for secondary nucleation polymerization (Nat. Prot. 11, 252- 272 (2016)), twice as many data points were used to arrive at similar conclusions.

Ans. We thank the reviewer for this important comment. To increase the number of data points, we performed aggregation of higher concentrations and lower concentrations. As mentioned above, the threshold concentration for DHS formation is 15 μM, and the concentrations higher than 35 μM such as 40 μM, we notice that the aggregation is so rapid and the solution also precipitates rapidly, which leads to the missing of some data points. Thus, we report a total of 5 concentrations, 15 μM, 20 μM, 25 μM, 30 μM and 35 μM for the fitting into secondary nucleation (Figure 4b,c).

This data is included in the revised manuscript as Figure 4b,c

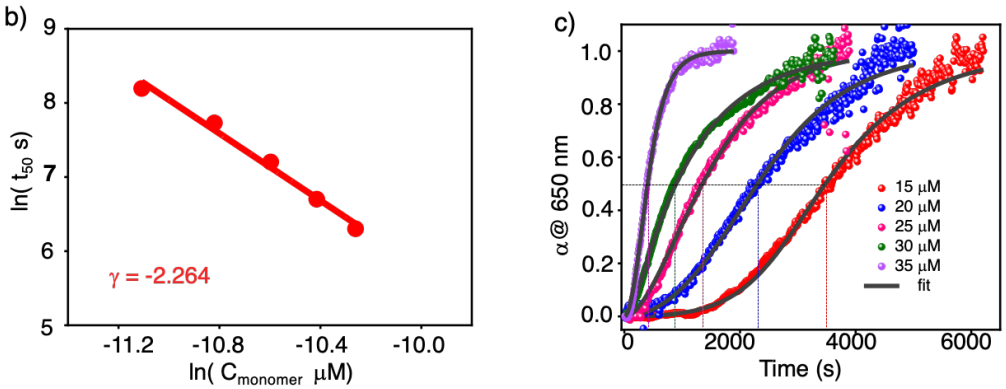

Figure 4. (b) double logarithmic plot of concentration and half-time of ***S*-G** at concentrations of 15 μM, 20 μM, 25 μM, 30 μM and 35 μM showing a linear fit. The slope gives the value of scaling exponent (γ) to be -2.264. (c) Kinetic profiles of aggregation of a 15 μM, 20 μM, 25 μM, 30 μM and 35 μM solutions in 15% $CHCl_3$ in IPA and corresponding fit in secondary nucleation dominated-unseeded, shows increasing lag time with decreasing concentration of ***S*-G**. Here α @650 nm represents the degree of supramolecular polymerization monitored at 650 nm.

The following sentences were included in the revised manuscript in page 7, bottom paragraph.

"We found that 15 μM is the threshold concentration because, at 10 μM, no significant changes in the absorption spectra were observed even for 3 hours at 25 °C (Supplementary Figure 25). Above 35 μM, such as 40 μM, temporal self-assembly is rapid. Hence we have analyzed the growth kinetics for five different concentrations (15 μM to 35 μM) by monitoring the absorbance at 650 nm wavelength."

6. It would also be beneficial to study the influence of temperature on the formation of the superstructures.

Ans. We thank the reviewer for suggesting us to include the effect of temperature. We studied the effect of temperature on the formation of DHS by monitoring the kinetics at temperatures ranging from 15 °C to 30 °C. At 15 C, the lag phase is reduced, and rapid assembly takes place(Supplementary Figure 28a). In this case as well DHS structures were obtained but with lesser dimensions. In stark

contrast, at 30 °C, aggregation takes place very slowly. Even after 6000 seconds, very less decrease in the absorbance is seen indicating that DHS formation is hampered.

This information is now included in the revised manuscript as Supplementary Figure 28.

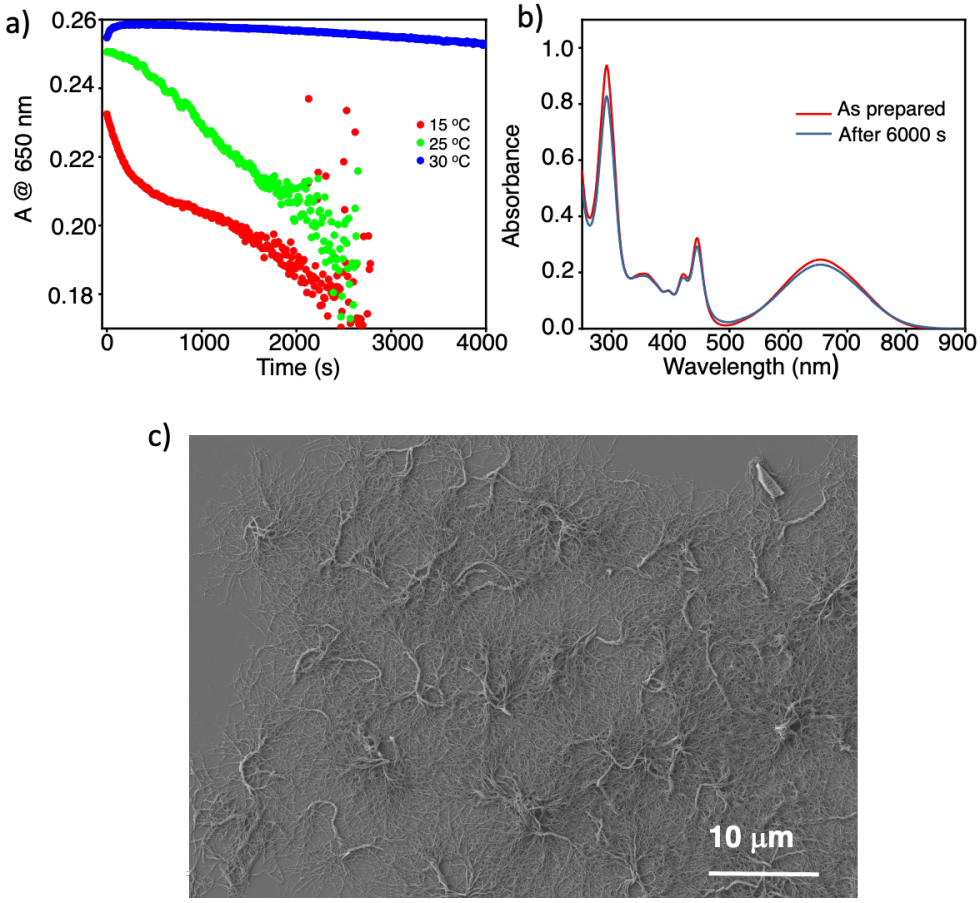

Supplementary Figure 28. (a) Influence of temperature on the aggregation kinetics of a 30 μM solution of ***S*-G** in 15% $CHCl_3$ in IPA at temperatures of 15 °C, 25 °C and 30 °C. (b) Comparison of absorption spectra of freshly prepared solution of ***S*-G** and after 6000 seconds, when kept at 30 °C. (c) FE-SEM image of a 30 μM solution of ***S*-G** in 15% $CHCl_3$ in IPA at 15 °C, spin-coated on silicon wafer.

The following sentences are included in the revised manuscript in page 10, bottom paragraph.

"We have also investigated the effect of temperature on DHS formation and depolymerization into monomers. At 25 °C, for a 30 μM solution of ***S*-G** in 15% $CHCl_3$ in IPA, DHS were obtained in 48 minutes. When cooled to lower temperatures, such as 15 °C, the assembly became rapid and completed in less than 30 minutes (Supplementary Figure 28a,c). However, the DHS obtained were smaller in size (Supplementary Figure 28c). At higher temperatures such as 30 °C, even after 3 hours, no significant decrease in absorbance at 650 nm, indicating that DHS formation is hampered (Supplementary Figure 28a,b). Even after 6000 seconds, very little decrease in the absorbance is seen (Supplementary Figure 28b)."

7. It is exciting to see the application of amylofit in supramolecular polymers. However, the procedures need to be performed very carefully. The discussion and conclusion based on amylofit are not convincing to me as the following questions: 1) a very important factor that can significantly influence the kinetical experiment is to exclude the existence of any small aggregates as it can remarkably

change the observed kinetics. The samples prepared in this work were by diluting a 1 mM stock solution of S/R-G in $CHCl_3$. Dilution is not a way to remove kinetic trapped aggregates, for this reason, it is very important to make sure there are no aggregates existing in 1 mM $CHCl_3$ solution. Variable concentration experiments in $CHCl_3$ (UVvis or HNMR) should be conducted to exclude the possibility.

Ans. We thank the reviewer for appreciating the application of Amylofit to Supramolecular polymers. We also thank you for pointing out the importance of initial control of sample preparation. We have updated the sample preparation methods in the main text as such to bring about more clarity.

To understand if smaller aggregates were still present even after dilution, we performed a concentration dependant absorbance of ***S*-G** in $CHCl_3$. For this purpose, we used concentrations of 100 µM, 133.5 µM, 166.6 µM, 200 µM, 233 µM, 266 µM and 300 µM. These are the concentrations formed when stock solution is diluted in $CHCl_3$, before the addition of IPA, hence monomeric nature of these concentrations is highly important. A plot of absorbance at 650 nm versus the concentration of ***S*-G** shows a linear dependence (R^2 value =0.99605), indicating the applicability of Beer–Lambert law, thus enabling us to conclude the monomeric nature of all these solutions (Supplementary Figure 35). If this were not true, we could expect a diversion from the linear trend at higher concentrations.

This information is now included in the revised manuscript as Supplementary Figure 35

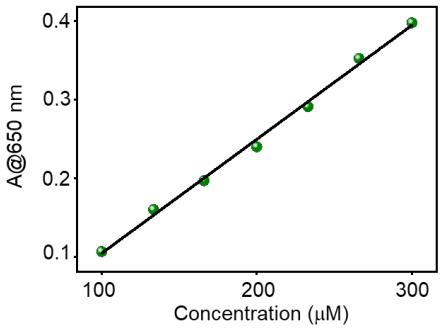

Supplementary Figure 35. A plot of absorbance at 650 nm versus the concentration of ***S*-G** in $CHCl_3$, (concentrations ranging from 100 µM to 300 µM) shows a linear dependence indicating the absence of aggregates in $CHCl_3$. These are the concentrations formed when the stock solution is diluted by adding $CHCl_3$ before the addition of IPA to prepare DHS.

The following sentences are included in the methods section, DHS preparation of the revised manuscript.

"Concentration dependent experiments of ***S*-G** by varying the concentration from 100 µM to 300 µM performed in $CHCl_3$ using UV-Vis absorption spectroscopy revealed a linear relation (Supplementary Figure 35), indicating the absence of any preexisting aggregates of ***S*-G/*R*-G** in $CHCl_3$ solution before the addition of IPA."

8. A clear biphasic behavior was observed in the kinetic profiles of aggregation at the concentrations of 30 uM and 35 uM. Those often come from poor control of initial conditions which further increase my first concern that small aggregates existed in the stock solution. One also should notice that these data are unsuitable for the fitting analysis.

Ans. We thank the reviewer for this very important comment. We realise the fact the biphasic nature at higher concentrations, such as 30 µM and 35 µM is aroused due to improper mixing of IPA when introduced into $CHCl_3$ containing the monomer. We have rectified this mistake in the revised manuscript with the data obtained by properly mixing the IPA and $CHCl_3$. The newly obtained data for 30 µM and 35 µM has no biphasic behaviour and showed a good fit into the secondary nucleation

model (Figure 4b,c and Supplementary Table 1). Moreover, in the methods section for DHS preparation, we have mentioned that "IPA added to $CHCl_3$ and mixed well".

The new data is added in the revised manuscript as Figure 4b,c and Supplementary Table 1. We have also updated the main text with new half-time values, MSE and scaling exponent (See main text page 7, bottom paragraph).

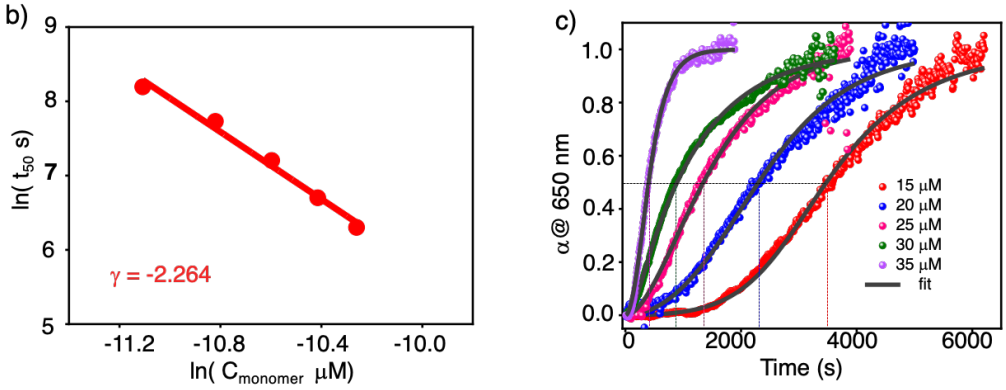

Figure 4. (b) double logarithmic plot of concentration and half-time of ***S*-G** at concentrations of 15 μM, 20 μM, 25 μM, 30 μM and 35 μM showing a linear fit. The slope gives the value of scaling exponent (γ) to be -2.264. (c) Kinetic profiles of aggregation of a 15 μM, 20 μM, 25 μM, 30 μM and 35 μM solutions in 15% $CHCl_3$ in IPA and corresponding fit in secondary nucleation dominated-unseeded, shows increasing lag time with decreasing concentration of ***S*-G**. Here α @650 nm represents the degree of supramolecular polymerization monitored at 650 nm.

Supplementary Table 1. Comparison of MSE of Secondary nucleation dominated unseeded versus primary nucleation in aggregation kinetics of ***S*-G.**

Concentration	MSE (Secondary nucleation dominated, unseeded)	MSE (primary nucleation)
15 μM	0.0009308	0.01592
20 μM	0.00161	0.007131
25 μM	0.001430	0.0022672
30 μM	0.0006945	0.00116
35 μM	0.0004	0.00166

9. I think that the support for the conclusion that "The absence of curvature in the linear fit suggests that it should align well with the secondary nucleation mechanism" is weak. First of all, the linear fitting in my opinion is very poor (let alone the high concentration data are not reliable). Secondly, a more intuitive conclusion based on this experiment is that it is negative curvature, indicating that competition exists. Thirdly (and again), at least 8-10 sets of data need to be obtained to get a reliable and accurate scaling exponent value.

Ans. We thank the reviewer for highlighting the importance of linear fit and curvature. We realise that in the previously reported data slight negative curvature was present, which can indicate the

presence of competitive processes such as secondary nucleation and fragmentation. We realized that this has arisen due to the biphasic behaviour of 30 uM and 35 uM solution (due to improper mixing of IPA and $CHCl_3$) and less number of concentrations used for the fit. Upon inclusion of new data for 15 uM, 30 uM, 35 uM, the newly obtained Log-Log plot showed a good linear fit without any curvature. Please see the response to comment 8 (above comment).

Additional comments

10. The FE-SEM images presented in this manuscript are spectacular. However, to further demonstrate the concept of "dendritic homochiral superstructures", AFM is required to investigate the helicity of branch fibers.

Ans. To investigate the homochirality of DHS, we performed AFM of the DHS at different locations of DHS to prove the homochirality. As can be seen by the AFM images, the central superhelix, the branching the end fibers etc. all follow same chirality. These images are further supported by the FE-SEM images. DHS formed from ***S*-G** have right-handed helical organization and the DHS of ***R*-G** have left-handed helical organization.

This new data is added to the revised manuscript as Supplementary Figures 19 and 20.

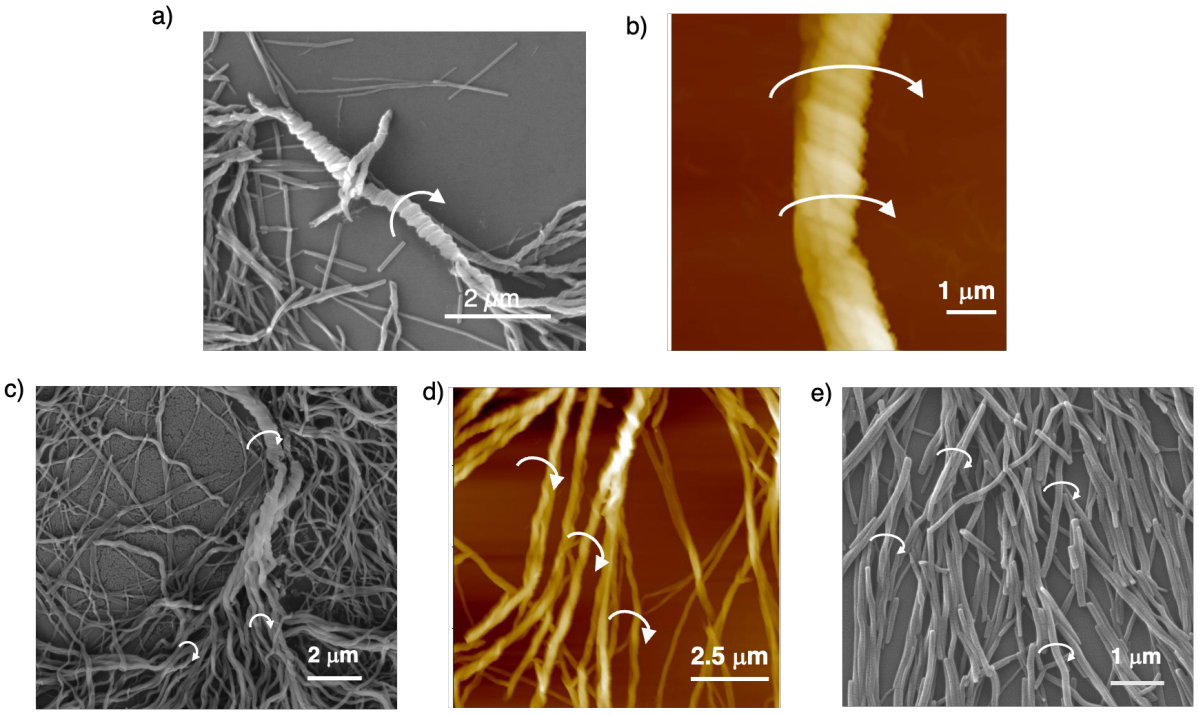

Supplementary Figure 19. FE-SEM and AFM images of DHS of ***S*-G** showing righthanded homochirality. (a) FE-SEM and (b) AFM images of superhelix of DHS of ***S*-G**. (c) FE-SEM image of branches in DHS showing righthanded helicity. (d) AFM and (e) FE-SEM images of thin helical fibers of DHS. These samples are prepared by spin-coating a 30 µM solution of ***S*-G** in 15% $CHCl_3$ in IPA on a silicon wafer.

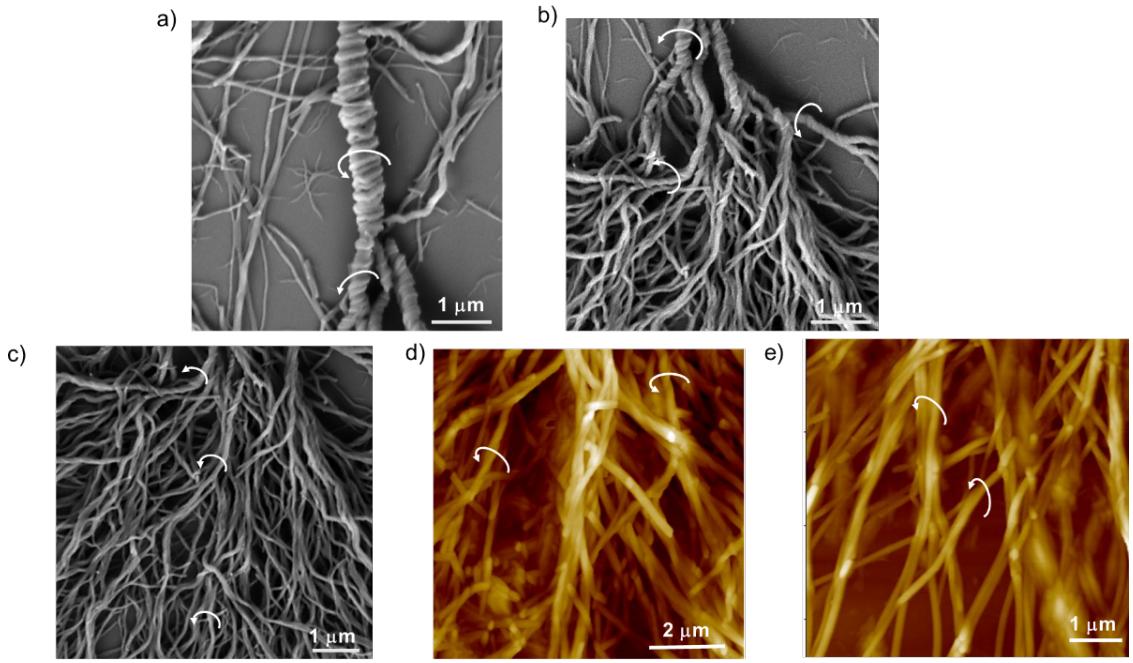

Supplementary Figure 20. FE-SEM images and AFM images of DHS of ***R*-G** showing lefthanded chirality and homochirality. (a) FE-SEM image of superhelix of DHS of ***R*-G**. (b) FE-SEM image of branches of DHS of ***R*-G**. (c) FE-SEM image of branches and thin fibers showing homochirality in DHS of ***R*-G**. (d) and (e) AFM images of thin helical fibers of DHS. These samples are prepared by spin-coating a 30 µM solution of ***R*-G** in 15% $CHCl_3$ in IPA on a silicon wafer.

The following sentences are included in the revised manuscript on page 6, top paragraph.

"Further analysis of FE-SEM and atomic force microscopy (AFM) images revealed that the central superhelix and branched thin helical fibers formed from ***S*-G** have a right-handed helical orientation (Supplementary Figure 19). Similarly, FE-SEM and AFM images revealed the left-handed helical orientation for DHS formed from of ***R*-G** (Supplementary Figure 20). These observations not only confirm the opposite helicity of DHS formed from ***S*-G** and ***R*-G** but also their homochiral nature."

11. Can the aggregates be 'reset' to the monomeric state via heating (VT curves) or sonication?

Ans. We thank the reviewer for this interesting suggestion. Accordingly, the DHS solution was subjected to sonication, and their absorption spectra were recorded after 5 and 15 minutes. However, the absorption spectra resemble more like DHS but not its monomeric form in $CHCl_3$ (Supplementary Figure 30). The TEM images of the sonicated sample reveals the fragmentation of DHS into superhelix and helical fibers. This indicate that DHS cannot be dissociated into monomers via sonication.

This information is now included in the revised manuscript as Supplementary Figure 30.

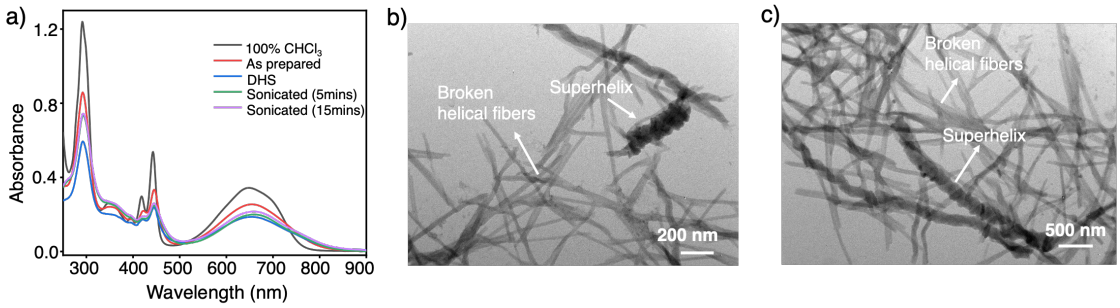

Supplementary Figure 30. (a) Effect of sonication on the absorption spectrum of DHS. Sonication for 5 minutes and 15 minutes increased the absorbance of DHS but it does not resemble the monomeric state. (b) and (c) TEM images of morphology after sonication for 15 minutes shows broken branched fibres and broken superhelix.

The effect of heating on DHS was studied by subjecting the DHS formed to slowly increasing temperature from 25 ºC to 65 ºC. Upon increasing the temperature, the absorbance of DHS increases, but it does not resemble monomeric absorbance in 100% $CHCl_3$. The morphology found at 65 ºC is small 1D helical fibers (Supplementary Figure 29f). The VT curves recorded for the heating of DHS at 1K/min shows a scattered spectra due to large particles in the solution. Thus by heating to 65 °C, DHS were fragmented into small helical fibers but not dissociated into monomers.

This information is now included in the revised manuscript as Supplementary Figure 29.

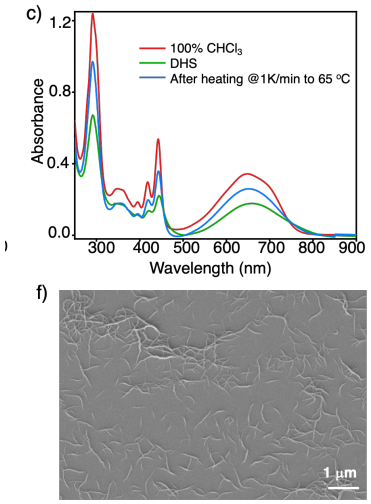

Supplementary Figure 29. (c) Absorption spectra of DHS of ***S*-G** and its comparison with 100 % $CHCl_3$. Upon heating, this solution does not go back to the monomeric state. (f) FE-SEM image obtained by spin-coating the hot solution of DHS solution, which was heated to 65 ºC.

The following sentences regarding stability of DHS to high temperature and sonication are added to the revised manuscript in page 11, top paragraph.

“Similarly, after the formation of DHS (30 µM), the solution was heated at 65 °C, but complete depolymerization was not observed (Supplementary Figure 29c). When this hot solution was spin-coated on a silicon wafer and visualized using FE-SEM, short helical fibres were observed (Supplementary Figure 29f). This indicates that in 15% $CHCl_3$ in IPA at 65 °C, DHS can be dissociated into short helical fibres but not completely into monomers. When the DHS solution was sonicated for 15 minutes, they were also not fully depolymerized into monomers, as evidenced by the absorption spectra but fragmented into superhelix and helical fibres (Supplementary Figure 30).”

12. Did the authors check if in-solution IR be used to follow the change in functional groups and subsequently determine the driving force of assembly?

Ans. We thank the reviewer for this suggestion. Accordingly, we have measured the IR spectra of ***S*-G** (30 µM). However, we could not find any signal corresponding to the ***S*-G**, probably due to low concentration. Even for the 100 µM solution also we could not find the signals. Hence we could not probe the formation of DHS in solution using IR.

13. Figure 1 is misleading since it displays that aggregation only starts on a surface while Figure 2C clearly shows that aggregation is also happening in solution.

Ans. We thank the reviewer for finding the mistake in Figure 1b. In Figure 1b of the main text, we have shown that the growth starts from the surface of a pre-existing fiber, which is already present in a solution. The same is reflected in Figure 2c. For better understanding, we have updated the schematic in Figure 1 in the revised manuscript.

The revised Figure 1 is given below for your reference.

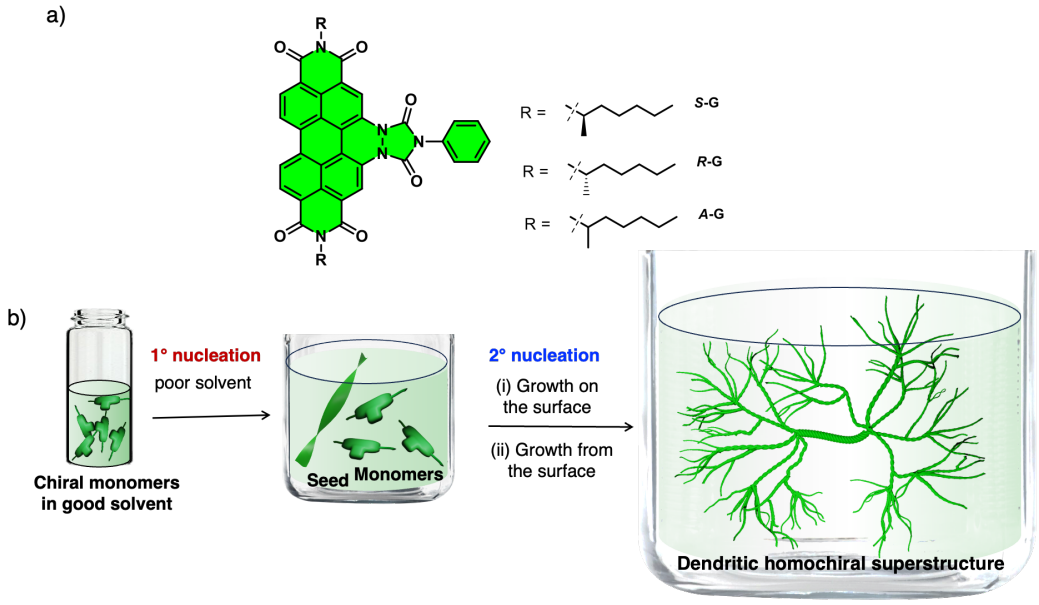

Figure 1. a) Molecular structures of NIR triimides having chiral (***S*-G** and ***R*-G**) and achiral alkyl (***A*-G**) side chains. b) schematic illustration of the formation of dendritic homochiral superstructures via 'growth on the surface' and 'growth from the surface' secondary nucleation-elongation process.

14. Figure 2: 4 different periods are used in the figures which makes it more difficult to compare that it should be. Also, why was it chosen to have for 2B only a window of 25 minutes? Was the CD signal decreasing after 25 minutes due to it potentially crashing out of solution

Ans. The 4 different time periods shown in Figure 2 of main text, i.e 0 minute, 15 minutes, 30 minutes and 45 minutes have no specific relation to UV-Vis spectrum or CD spectrum. These 4 different time intervals have been chosen to identify the macroscopic changes happening in the solution at equal time intervals that eventually result in the formation of DHS. These same-time intervals are used to prepare FE-SEM samples, as shown in Figure 5.

Yes. The CD signal decreased after 25 minutes due to DHS crashing out of the solution. This has been now mentioned in the revised manuscript.

The following sentence is modified in the revised manuscript, page 5, middle paragraph.

"As a result, a reduction in the CD signal after 25 minutes was observed due to the crashing of self-assembled structures out of the solution."

15. Were Linear dichroism (LD) measurements considered to determine the starting point of aggregation? 1D polymer cannot display an LD signal while aggregates will. LD should also be performed to know if LD contributes to the CD signals obtained in the manuscript. On the other hand, it will be interesting to see if preferential oriented supramolecular polymers were formed in solution after 25 mins.

Ans. We thank the reviewer for this interesting suggestion. Accordingly, we have recorded the time-dependent LD spectra. Although the LD signal was weak, no significant increase was observed up to 5 minutes. After 5 minutes, the LD signal increased and saturated after 20 minutes. These observations indicate that bigger aggregates start to form after 5 minutes and weak LD signal even after 20 minutes indicate the preferential orientation of supramolecular polymers in solution is low. Moreover, the CD signal obtained might have some contribution from LD as well.

This information is now included in the revised manuscript as Supplementary Figure 17.

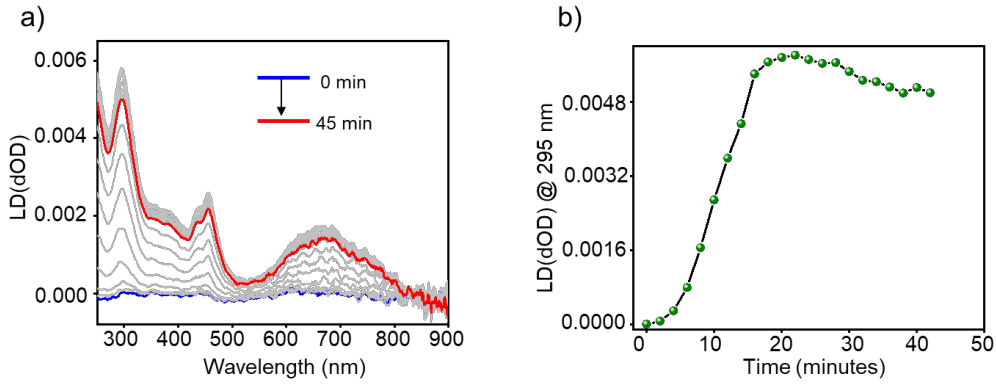

Supplementary Figure 17. (a) Time dependant linear dichroism spectra of a 30 µM solution of ***R*-G** in 15 vol% $CHCl_3$ in IPA monitored over a time period of 45 minutes. (b) A plot of variation of LD signal at 295 nm versus time.

The following sentences regarding LD are added to the main text, page 5, middle paragraph.

"We have also performed time dependent linear dichroism (LD) measurements to understand its contribution to the CD signal and preferential orientation of SPs in solution. Although the LD signal is weak, we have seen a significant increase after 5 minutes and saturation after 25 minutes (Supplementary Figure 17). Hence, the contribution of the LD signal to the CD signal is low, and the resultant SPs have some degree of preferential orientation in the solution."

16. The IR of the enantiomers differs quite considerably which seems odd

Ans. We thank the reviewer for finding the mistake in our IR data. The IR reported in the previous version has a contribution from CO_2 gas in the sample chamber. We have re-recorded the IR spectra of triimides by purging the chamber with N_2, and now they look very similar.

The manuscript is updated with the revised data, and it is given below for your reference.

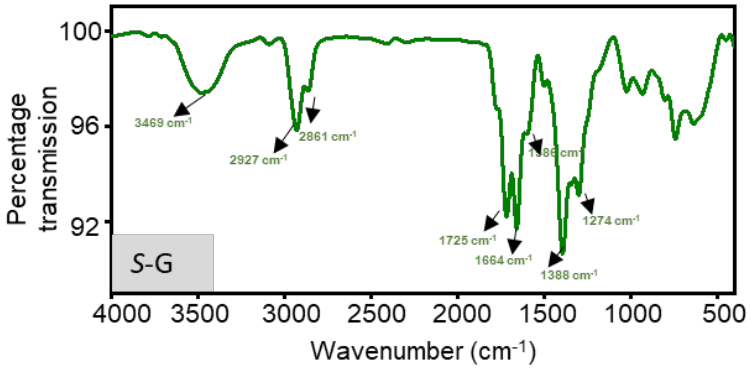

Supplementary Figure 3. FTIR spectrum of ***S*-G**. The peak near 3600 cm^{-1} is due to the presence of moisture in the KBr pellet. The peaks at 2927 cm^{-1} and 2861 cm^{-1} are due to the alkyl C-H stretching, 1725 cm^{-1} and 1664 cm^{-1} are due to carbonyl stretching (C=O), peak at 1586 cm^{-1} is due to aromatic C=C stretching, 1274 cm^{-1} is due to C-N stretching.

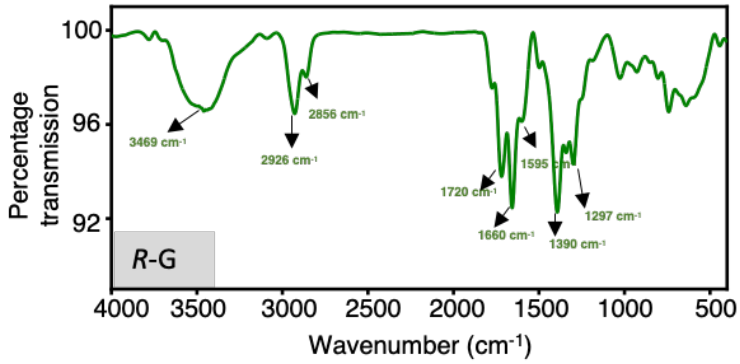

Supplementary Figure 7. FTIR spectrum of ***R*-G** in KBr pellet. The peak near 3600 cm^{-1} is due to the presence of moisture in the KBr pellet. The peaks at 2926 cm^{-1} and 2858 cm^{-1} are due to the alkyl C-H stretching, 1723 cm^{-1} and 1663 cm^{-1} are due to carbonyl stretching (C=O), peak at 1588 cm^{-1} is due to aromatic C=C stretching, 1287 cm^{-1} is due to C-N stretching.

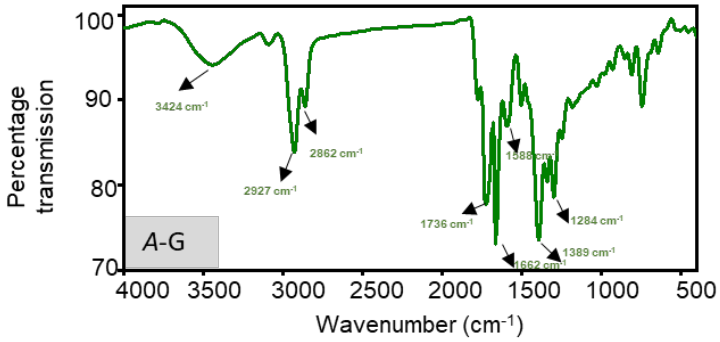

Supplementary Figure 11. FTIR spectrum of ***A*-G** in KBr pellet. The peak near 3600 cm^{-1} is due to the presence of moisture in the KBr pellet. The peaks at 2927 cm^{-1} and 2862 cm^{-1} are due to the alkyl C-H stretching, 1736 cm^{-1} and 1662 cm^{-1} are due to carbonyl stretching (C=O), peak at 1588 cm^{-1} is due to aromatic C=C stretching, 1284 cm^{-1} is due to C-N stretching.

17. Figure S12: what is the difference between A and B?

Ans. The TEM images shown in Figure S12 (Now Supplementary Figure 18) correspond to the 30 μM solution of ***S*-G** in 15% $CHCl_3$ in IPA at 0 minutes (freshly prepared). These two images were taken at two different areas of the TEM grid of the same sample. This has been now mention in the figure caption of Supplementary Figure 18.

Reviewer 2

1. In this manuscript, the authors report the non-covalent synthesis of dendritic purely chiral superstructures by a secondary nucleation extension process using NIR triimide dyes as building blocks. The analysis of the kinetics and time evolution of the morphology shows that the formation of dendritic homochiral superstructures proceeds via growth on the surface and growth from the surface of the crystal species. The combination of these two processes leads to the formation of elegant homochiral superstructures with dimensions of about 0.4 mm2, with a superhelix at the center and helical fibers as branches. Moreover, these dendritic homochiral superstructures exhibit significantly high chiral optical photoresponse with gfactor sizes reaching values up to 0.55-0.6. This work is original and well-organized, and I recommend to accept this manuscript for publication in Nature Communications

   Ans. We thank the reviewer for nicely summarising our work and recommending it for publication in Nature Communications.

2. Since the self-assembly proceed in two stages: growth on the surface and growth from the surface. Is it possible to discerned the two stages from the absorption and CD spectra in Figure 2a and 2b

   Ans. We thank the reviewer for this interesting question. Growth on the surface and growth from the surface have taken place simultaneously from the beginning, which led to the formation of the DHS. We could not see any specific changes in absorption and CD spectra that can differentiate growth on the surface and growth from the surface processes. Hence it is not possible to distinguish these two processes using absorption and CD spectra.

3. From Figure 2c, the sample seems precipitated in 15 minutes during the self-assembly (30 μM, 15% CHCl3 in IPA). So, are the UV-vis and CD spectra recorded under the same conditions (30 μM, 15% CHCl3 in IPA, 0-48 minutes) reliable?

   Ans. We thank the reviewer for this important question. We have monitored the temporal self-assembly by probing the absorbance of the monomers at 650 nm. When the monomers are consumed to form DHS, a decrease in the absorbance is observed. The UV-Vis spectra obtained under these conditions are reliable because the decrease in the absorbance is due to a decrease in monomer concentration, which is not affected due to precipitation. Since monomers will be the solution and contribute to the absorbance, we have used the decrease in the concentration of monomers as a probe to study the temporal evolution of self-assembly. In contrast, only chiral assemblies are responsible for the CD signals. Thus, the leftover monomers do not have any contribution to the CD peaks obtained. The CD signal keeps increasing at 15 minutes time duration even though some precipitation is seen because monomers are still converting to aggregates. Hence, in this case, the initial increase in CD intensity up to 25 minutes is due to the consumption of monomers to form larger chiral assemblies. But after 25 minutes, the precipitation of larger chiral assemblies (DHS) is more dominant than the conversion of monomers into chiral assemblies. Hence, a decrease in the CD signal is observed after 25 minutes.

4. Since the monomers are pure chirality, the helicity of the self-assembled fibers is suggested to discuss? For example, how about the excess of one-handed helix of the supramolecular nanofibers? Or they self-assembled into a single left- or right-handed supramolecular helices? This is important to confirm the self-assemblies are real DHS

Ans. We thank the reviewer for this comment. To assess the helicity of the self-assembled fibers, microscopic techniques such as FE-SEM and AFM were used. As can be seen by the AFM and FE-SEM images, the central superhelix, the branching the end fibers etc. all follow same chirality. DHS formed from ***S*-G** have a right-handed helical organization and the DHS of ***R*-G** have left-handed helical organization. We have also performed co-assembly experiment by mixing different molar ratios of ***S*-G** and ***R*-G** and analysed the morphology (See Reviewer-2, commonet-8).

This new data is added to the revised manuscript as Supplementary Figures 19 and 20.

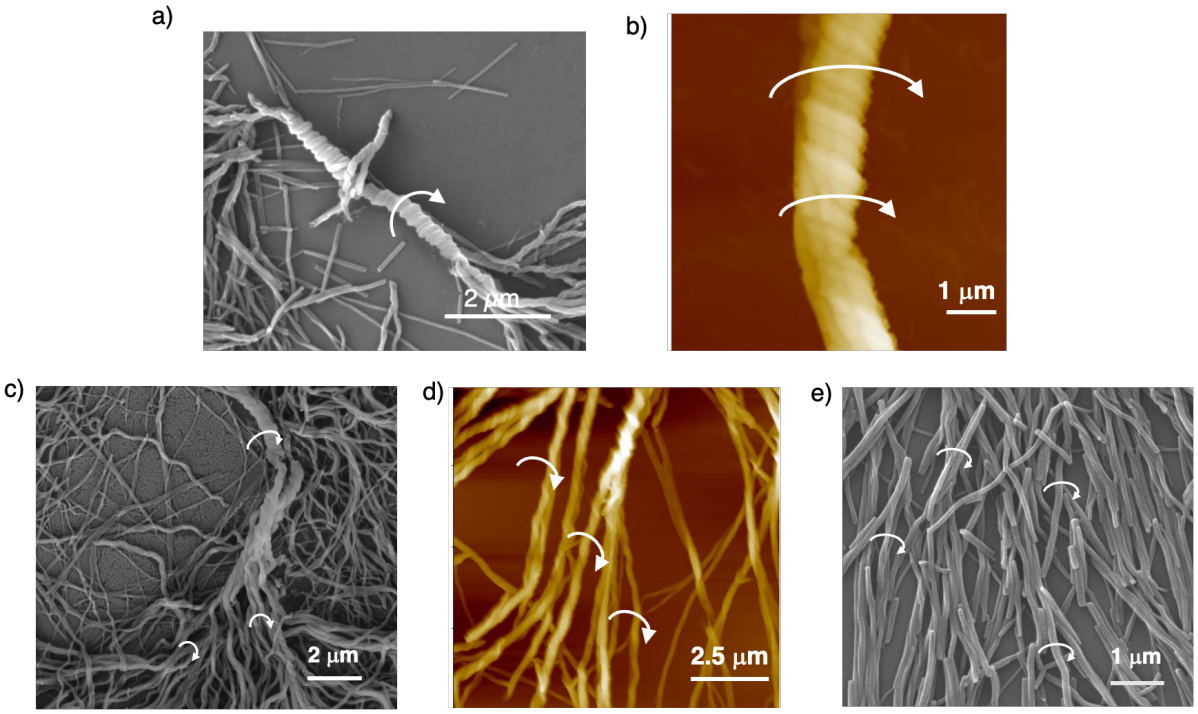

Supplementary Figure 19. FE-SEM and AFM images of DHS of ***S*-G** showing righthanded homochirality. (a) FE-SEM and (b) AFM images of superhelix of DHS of ***S*-G**. (c) FE-SEM image of branches in DHS showing righthanded helicity. (d) AFM and (e) FE-SEM images of thin helical fibers of DHS. These samples are prepared by spin-coating a 30 µM solution of ***S*-G** in 15% $CHCl_3$ in IPA on a silicon wafer.

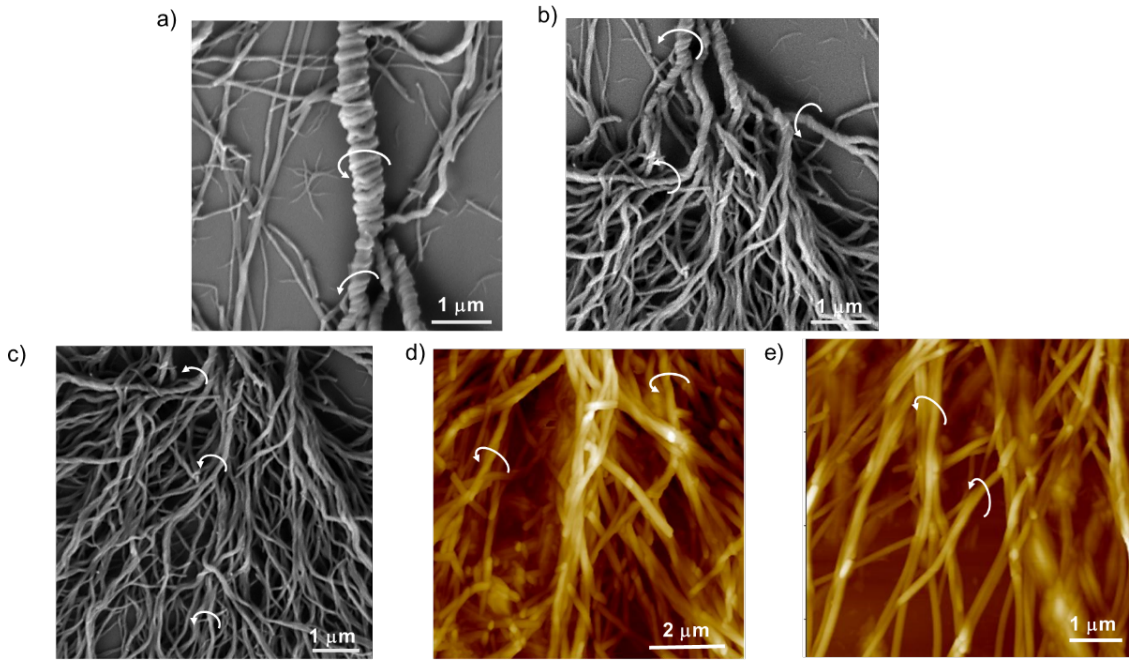

Supplementary Figure 20. FE-SEM images and AFM images of DHS of ***R*-G** showing lefthanded chirality and homochirality. (a) FE-SEM image of superhelix of DHS of ***R*-G**. (b) FE-SEM image of branches of DHS of ***R*-G**. (c) FE-SEM image of branches and thin fibers showing homochirality in DHS of ***R*-G**. (d) and (e) AFM images of thin helical fibers of DHS. These samples are prepared by spin-coating a 30 µM solution of ***R*-G** in 15% $CHCl_3$ in IPA on a silicon wafer.

The following sentences are included in the revised manuscript on page 6, top paragraph.

"Further analysis of FE-SEM and atomic force microscopy (AFM) images revealed that the central super helix and branched thin helical fibers formed from ***S*-G** have right-handed helical orientation (Supplementary Figure 19). Similarly, FE-SEM and AFM images revealed the left-handed helical orientation for DHS formed from of ***R*-G** (Supplementary Figure 20). These observations not only confirm the opposite helicity of DHS formed from ***S*-G** and ***R*-G** but also their homochiral nature."

5. Can the helical nanofibers directly emit CPL light

Ans. We thank the reviewer for this comment. In the present case the self-assembly of NIR triimides leads to the quenching of fluorescence (Supplementary Figure 15b). The fluorescence of helical nanofibers is negligible. Hence they may not show any CPL.

6. For comparison, the CD spectra of the self-assemblies of R-G are suggested to provide in Figure 2b in the main.

Ans. We thank the reviewer for this suggestion. The mirror image time-dependent CD spectra have now been added to Figure 2b. The updated Figure 2 is shown below for your reference.

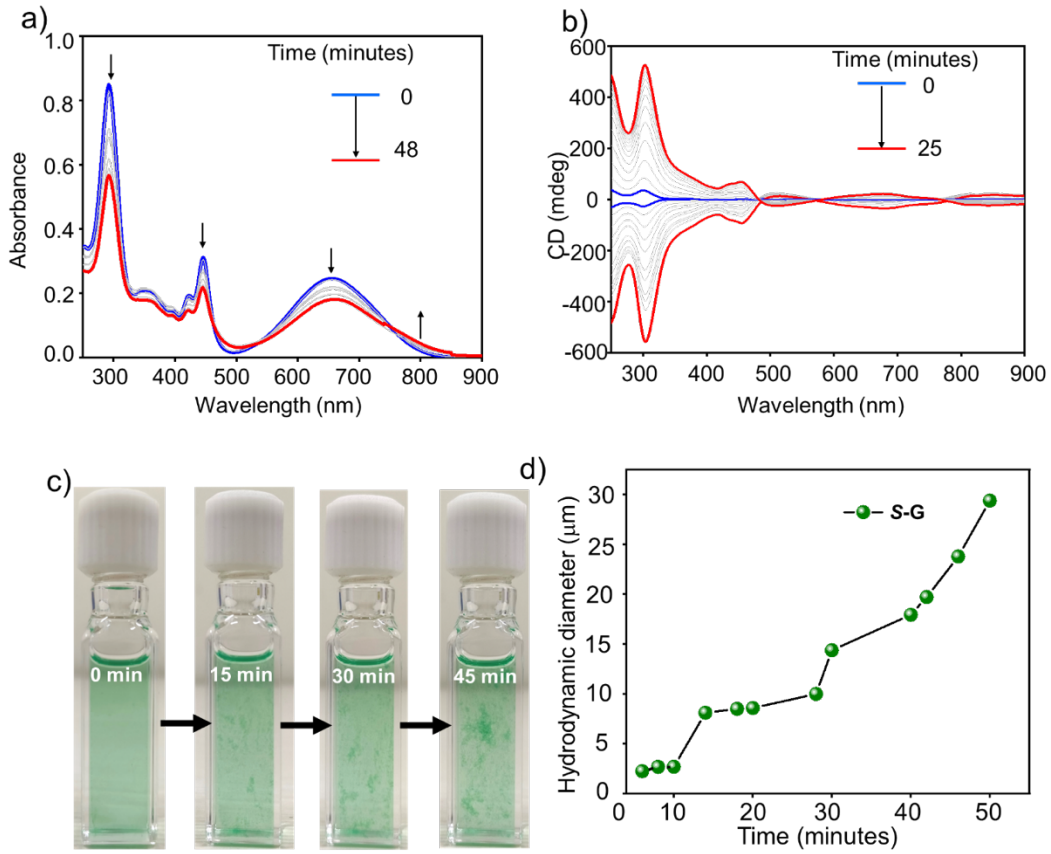

Figure 2. (a) Time dependant absorption spectra of 30 μM of ***S*-G** in 15% $CHCl_3$ in IPA over a period of 48 minutes representing its temporal growth. (b) Time dependant CD spectra of a 30 μM solution of ***S*-G** and ***R*-G** in 15% $CHCl_3$ in 85% IPA. (c) Photographs of solution of ***S*-G** (30 μM) in 15% $CHCl_3$ in IPA at different time intervals. (d) Time-dependent dynamic light scattering (DLS) data of ***S*-G** (30 μM) in 15% $CHCl_3$ in IPA.

7. For the UV-Vis absorption spectra (Figure 2a), the authors tested for 48 min while the CD spectra (Figure 2b) was only 25 minutes, could the authors please describe the reason for this?

Ans. We thank the reviewer for this query. The UV-Vis spectrum shows a continuous decrease in absorbance, which is due to conversion of monomers into DHS. This change is accompanied by an increase in the CD signal initially. As already discussed in one of the previous response (Response no.3, reviewer-2), CD spectra obtained is due to chiral assemblies because monomers are CD silent. But at a later stage, these chiral assemblies become big enough to come out of the solution, which leads to a decrease in CD signal. The CD spectra have been measured over a period of 48 minutes; the ellipticity at 650 nm versus the time plot is also shown in Supplementary Figure 16. This decrease after 25 minutes indicates DHS coming out of solution is dominating than monomers converting into DHS.

8. How about the self-assembly of S- and R-G in different molar ratios?

Ans. We thank the reviewer for this interesting suggestion. We analysed the self-assembly behaviour of different molar ratios of ***S*-G** and ***R*-G,** such as 1:1, 1:2 and 1:5. The growth of the aggregates has been monitored using CD spectrophotometry and FE-SEM imaging (Supplementary Figure 31). The results showed that fully developed DHS can be synthesized via secondary nucleation using pure chiral isomers (***S*-G** or ***R*-G**) but not by their mixture.

These results are now included in the revised manuscript as Supplementary Figure 31.

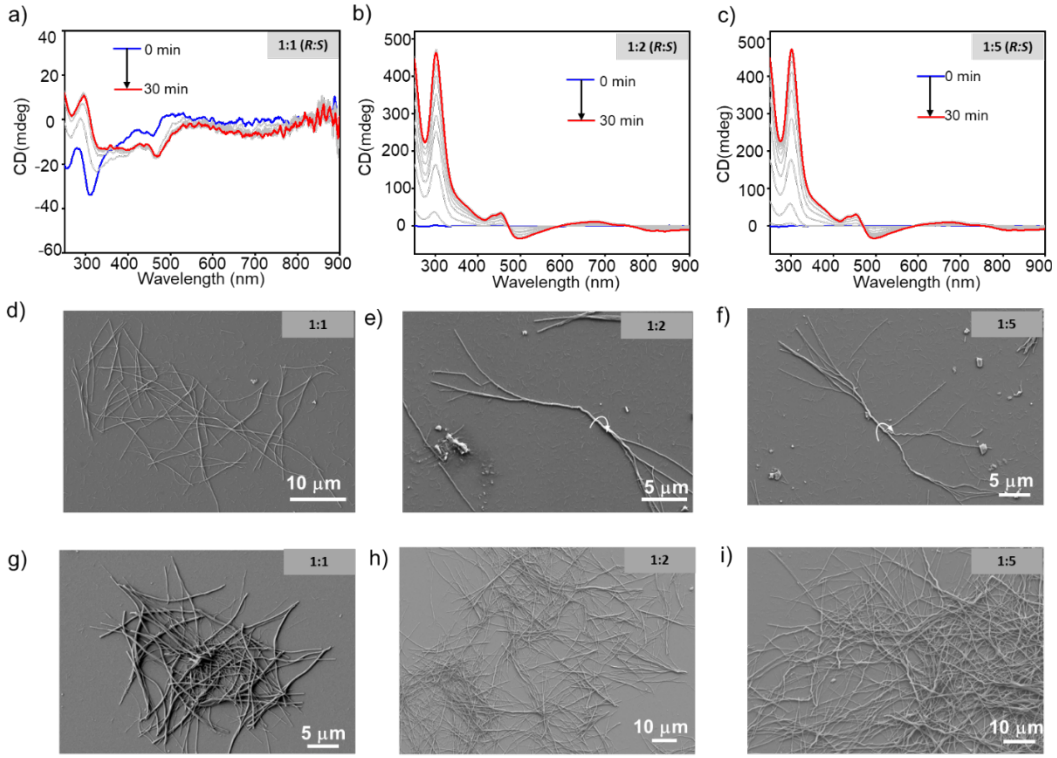

Supplementary Figure 31. Time dependant CD spectra of (a) 1:1, (b) 1:2 and (c) 1:5 mixtures of ***R*-G** and ***S*-G**. (d) and (g) FE-SEM images of 1:1 mixture of ***S*-G** and ***R*-G** spin-coated on a silicon wafer. (e) and (h) FE-SEM images of 1:2 mixture of ***S*-G** and ***R*-G** spin-coated on a silicon wafer. (f) and (i) FE-SEM images of 1:5 mixture of ***R*-G** and ***S*-G** spin-coated on a silicon wafer.

The following paragraph describing the results of mixing different molar ratios of ***S*-G** and ***R*-G** is included in the revised manuscript in page 11, second paragraph.

"To understand how the DHS formation will be affected by mixing different molar ratios of ***S*-G** and ***R*-G**, we have mixed them in their monomeric state in $CHCl_3$ in 1:1, 1:2 and 1:5 molar ratios before adding IPA (Supplementary Figure 31). The growth of the SPs has been monitored using CD spectroscopy and FE-SEM imaging. The equimolar mixture of ***S*-G** and ***R*-G** has negligible CD signal compared to homochiral aggregates and it is similar to ***A*-G** (Supplementary Figures 21c and 31a). FE-SEM images obtained after completion of the self-assembly process revealed the existence of 1D fibers similar to ***A*-G** but not DHS (Supplementary Figure 31d,g). When the ratio of ***R*-G** to ***S*-G** is changed to 1:2 (10 µM of ***R*-G** and 20 µM of ***S*-G)** and 1:5 (5 µM of ***R*-G** and 25 µM of ***S*-G)**, the CD signals obtained are slightly lower than pure ***S*-G** (Supplementary Figure 31b,c). The FE-SEM analysis of these samples indicated the presence of chiral SPs with branches, and DHS with less branching, but not fully developed DHS as seen in the case of pure ***S*-G** (Supplementary Figure 31e,f,h,i). Multiple areas were analysed to identify homochirality, and it was concluded that these helices are righthanded similar to SPs obtained from ***S*-G**. Hence, we conclude that fully developed DHS can be synthesized via secondary nucleation using pure chiral isomers (***S*-G** or ***R*-G**)."

9. Some important papers related to this paper closely are encouraged to cite, such as Chem. Sci. 2024, 15, 2946–2953. Acc. Chem. Res. 2023, 56, 2954-2967. Angew. Chem. Int. Ed. 2022, 61, e202207028. Angew. Chem., Int. Ed. 2020, 59, 16675–16682.

Ans. We thank the reviewer for suggesting some important references on the self-assembly chiral polymers.

These papers have been cited as references 38-41 in the revised manuscript

(38) Xu, L. et al. Crystallization-driven asymmetric helical assembly of conjugated block copolymers and the aggregation induced white-light emission and circularly polarized luminescence. *Angew. Chem. Int. Ed.* **59**, 16675–16682 (2020).
(39) Wang, C., Xu, L., Zhou, L., Liu, N. & Wu, Z. Q. Asymmetric living supramolecular polymerization: precise fabrication of one-handed helical supramolecular polymers. *Angew. Chem. Int. Ed.* **61**, e202207028 (2022).
(40) Liu, N., Gao, R. T., & Wu, Z. Q. Helix-induced asymmetric self-assembly of π-conjugated block copolymers: from controlled syntheses to distinct properties. *Acc. Chem. Res.* **56,** 2954-2967 (2023).
(41) Gao, R. T. et al. One-pot asymmetric living copolymerization-induced chiral self-assemblies and circularly polarized luminescence. *Chem. Sci.* **15,** 2946-2953 (2024).

Reviewer 3

1. In this work, the authors reported the formation of dendritic homochiral superstructures through the secondary nucleation of perylene diimide derivatives. The resulting superstructures consist of a superhelix center with helical fiber branches, covering an area of approximately 0.4 mm^2. While the optical images are visually appealing, the experimental details and discussions are insufficient. Consequently, this manuscript appears to report a phenomenon rather than providing scientific insights that would be valuable for peer researchers. Therefore, the manuscript is not suitable for publication in Nature Communications at this stage. The following issues need to be addressed:

Ans. We thank the reviewer for the critical comments on our manuscript. We have addressed all the comments by performing additional experiments and theoretical calculations. We hope that the revised manuscript will be suitable for *Nature Communications.*

2. The characterization of the chemical structures of S/R-G requires further enhancement. In the 1H NMR spectra, the corresponding peaks in S/R-G show shifts of approximately 0.3 ppm (e.g., 9.30 ppm vs 9.03 ppm). This raises concerns about whether the 1H NMR is properly calibrated; if it is, an explanation for these shifts should be provided.

Ans. We thank the reviewer for this important comment. We realize the mistake from our end regarding the irregularities in the NMR. This mismatch of values is due to the difference in the concentration of ***S*-G** and ***R*-G** in $CDCl_3$. The error has now been rectified by taking equal amount of solute (2.5 mg in 0.5 mL of $CDCl_3$) for NMR measurements of all three molecules- ***S*-G**, ***R*-G** and ***A*-G**. Here, ***A*-G** is achiral NIR triimide, which we have synthesized as per your suggestion (see comment-5, Reviewer-3).

The new ^{1}H-NMR spectra are included in the revised manuscript as Supplementary Figures 1, 5 and 9. These spectra are given below for your reference. We have also updated the ^{1}H-NMR values in the synthesis and characterization section of each molecule.

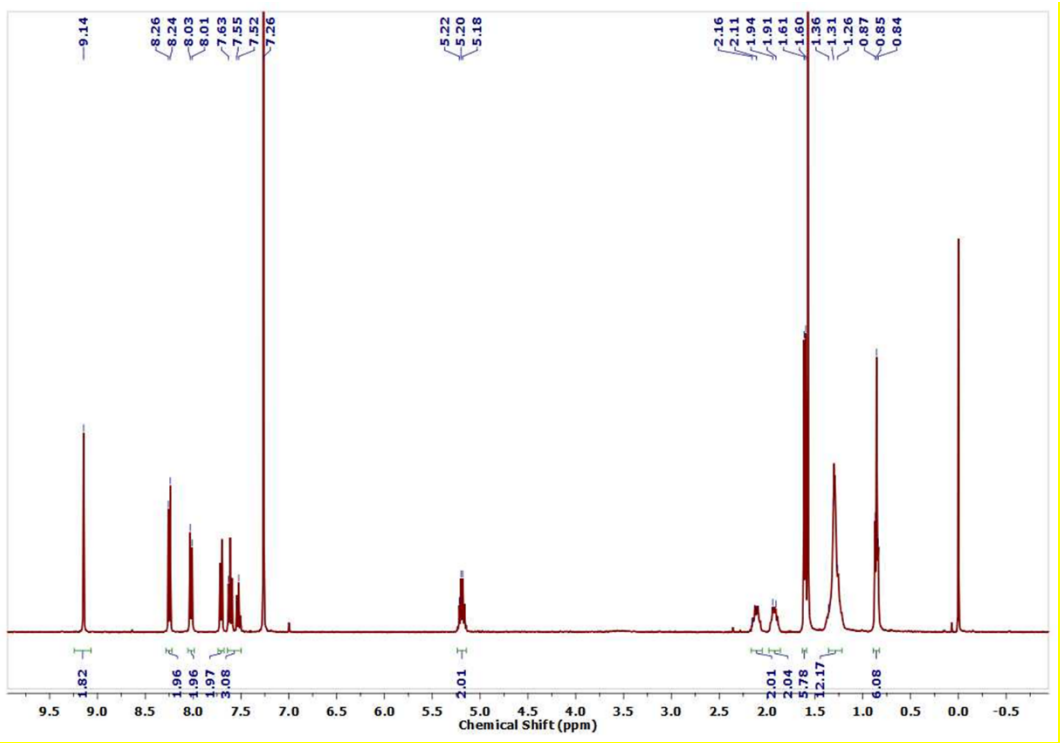

Supplementary Figure 1. ^{1}H-NMR spectrum of ***S*-G** in $CDCl_3$ (concentration: 2.5 mg in 0.5mL of $CDCl_3$).

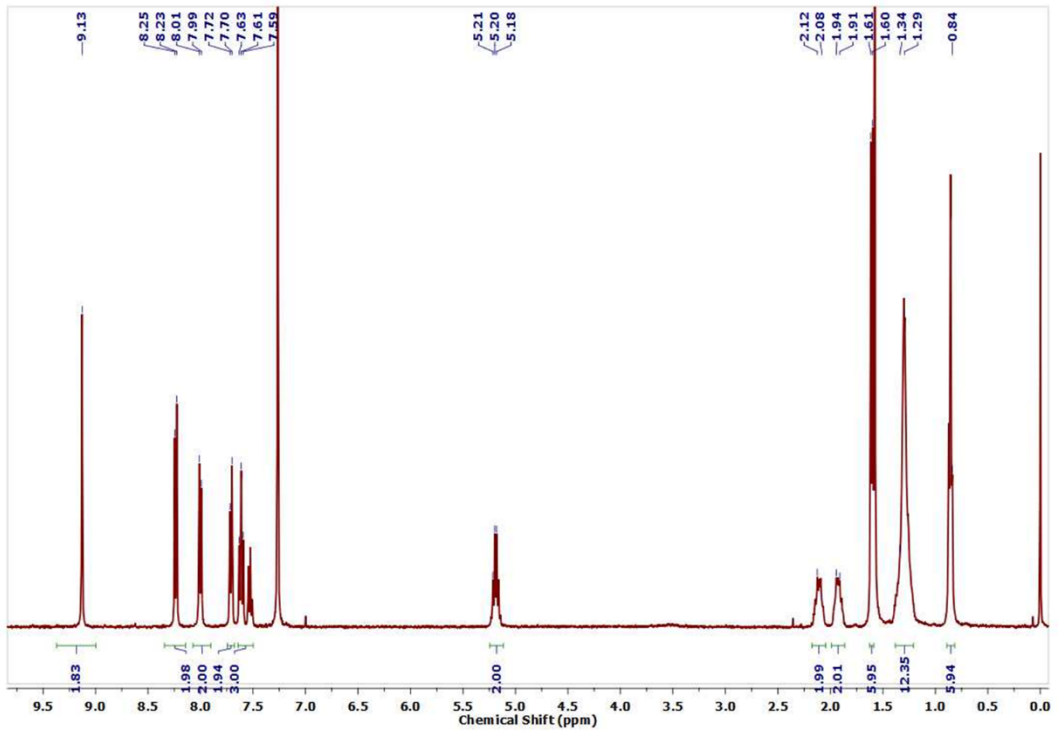

Supplementary Figure 5. ^{1}H-NMR spectrum of ***R*-G** in $CDCl_3$ (concentration: 2.5mg in 0.5 mL of $CDCl_3$).

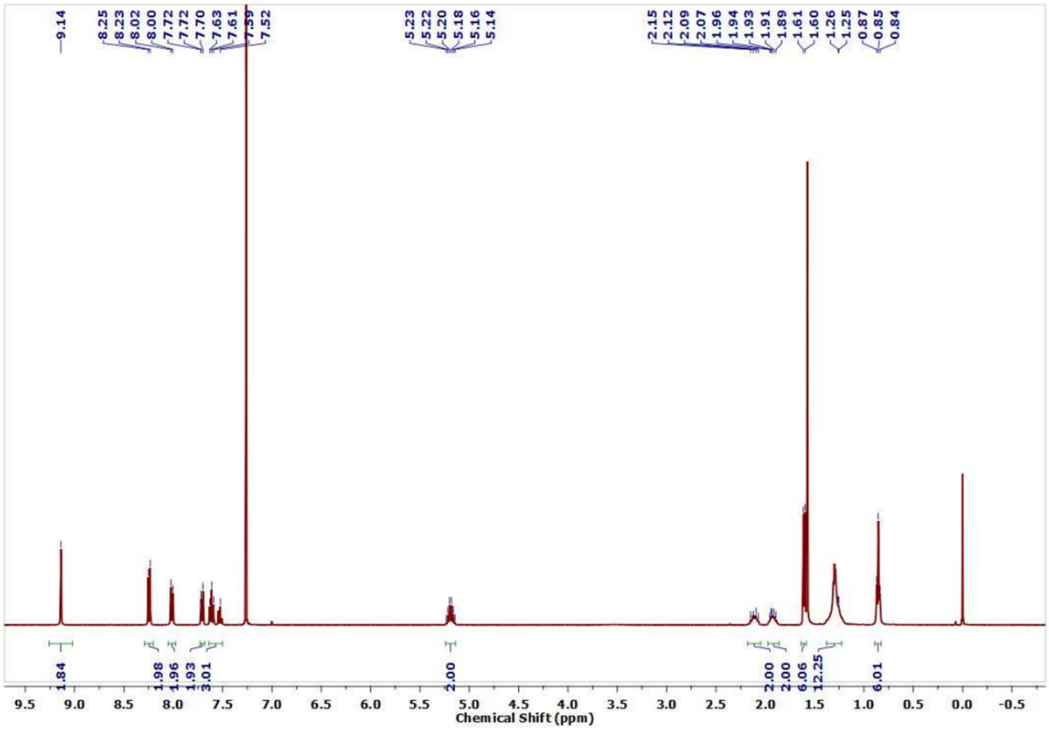

Supplementary Figure 9. ^{1}H-NMR spectrum of ***A*-G** in $CDCl_3$. (concentration: 2.5mg in 0.5 mL of $CDCl_3$).

3. The MALDI-TOF spectra should also include a zoomed-in view to clearly display the isotope patterns of the respective peaks.

Ans. We thank the reviewer for this suggestion. The zoomed-in MALDI-TOF spectra have been added as an inset to the existing data.

The new MALDI-TOF spectra are included in the revised manuscript as Supplementary Figures 4, 8 and 12. These spectra are given below for your reference.

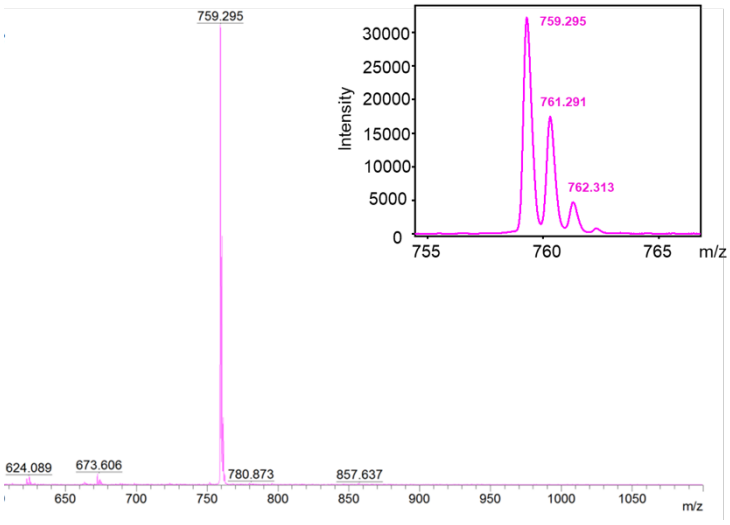

Supplementary Figure 4. MALDI-TOF Spectrum of ***S*-G**, (inset: zoomed in spectrum to show isotopic patterns).

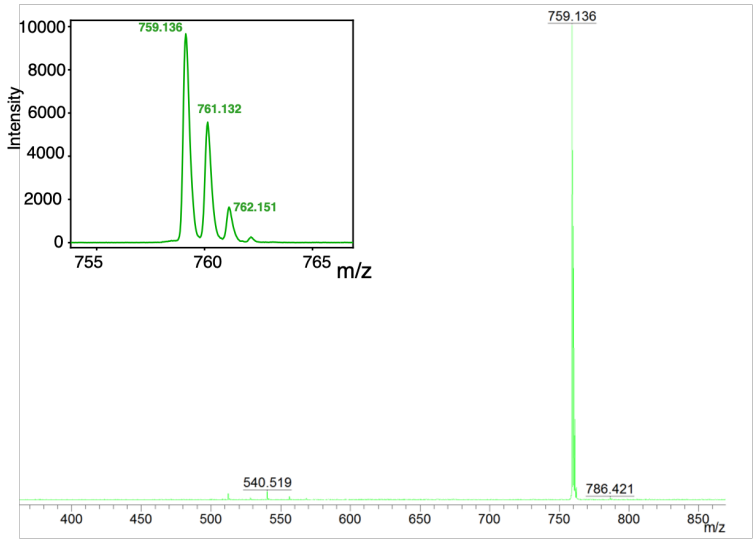

Supplementary Figure 8. MALDI-TOF Spectrum of ***R*-G** (inset: zoomed in spectrum to show isotopic patterns).

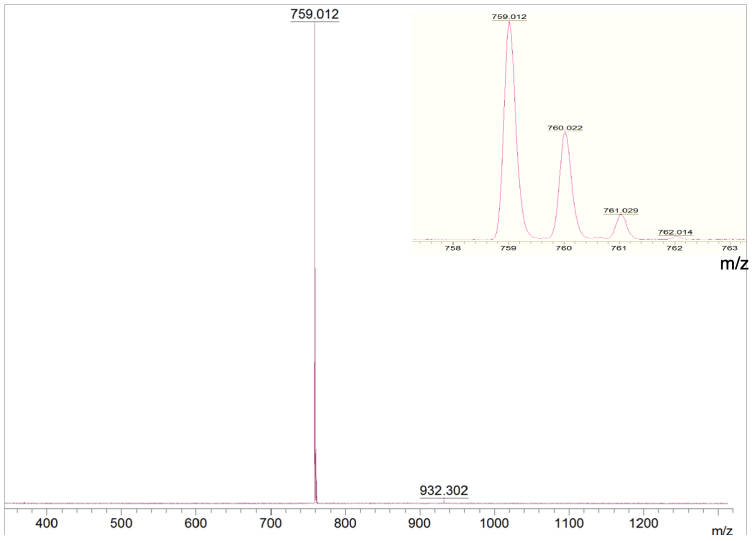

Supplementary Figure 12. MALDI-TOF Spectrum of ***A*-G** (inset: zoomed in spectrum to show isotopic patterns).

4. Additionally, the FTIR spectra of S-G and R-G differ significantly, with R-G exhibiting more intense peaks around 3500 cm^{-1}, which are unexpected and warrant explanation. Furthermore, S-G displays more pronounced C-O peaks around 2400 cm^{-1} compared to R-G, potentially indicating the presence of CO_2. This suggests that the quality of the FTIR data should be improved.

Ans. We thank the reviewer for finding the mistake in our IR data. The peaks at 3500 cm^{-1} in the FTIR spectrum of ***R*-G** is due to the presence of moisture in KBr pellet. The peaks at 2400 cm^{-1} in the FTIR of ***S*-G** is due to CO_2. The IR reported in the previous version has a contribution from CO_2 gas in the sample chamber. We have re-recorded the IR spectra of triimides by purging the chamber with N_2, and now they look very similar.

The new FT-IR spectra are included in the revised manuscript as Supplementary Figures 3, 7 and 11.

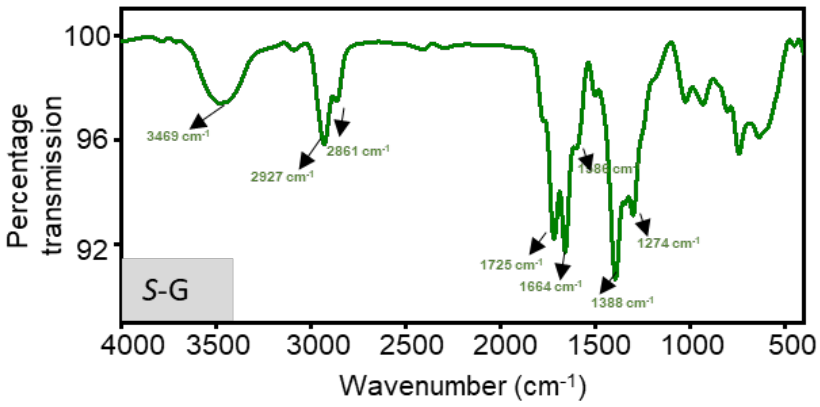

Supplementary Figure 3. FTIR spectrum of ***S*-G**. The peak near 3600 cm^{-1} is due to the presence of moisture in the KBr pellet. The peaks at 2927 cm^{-1} and 2861 cm^{-1} are due to the alkyl C-H stretching, 1725 cm^{-1} and 1664 cm^{-1} are due to carbonyl stretching (C=O), peak at 1586 cm^{-1} is due to aromatic C=C stretching, 1274 cm^{-1} is due to C-N stretching.

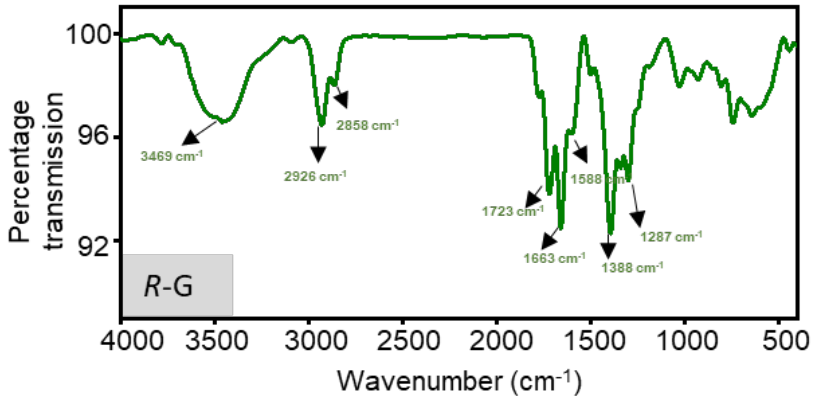

Supplementary Figure 7. FTIR spectrum of ***R*-G** in KBr pellet. The peak near 3600 cm^{-1} is due to the presence of moisture in the KBr pellet. The peaks at 2926 cm^{-1} and 2858 cm^{-1} are due to the alkyl C-H stretching, 1723 cm^{-1} and 1663 cm^{-1} are due to carbonyl stretching (C=O), peak at 1588 cm^{-1} is due to aromatic C=C stretching, 1287 cm^{-1} is due to C-N stretching.

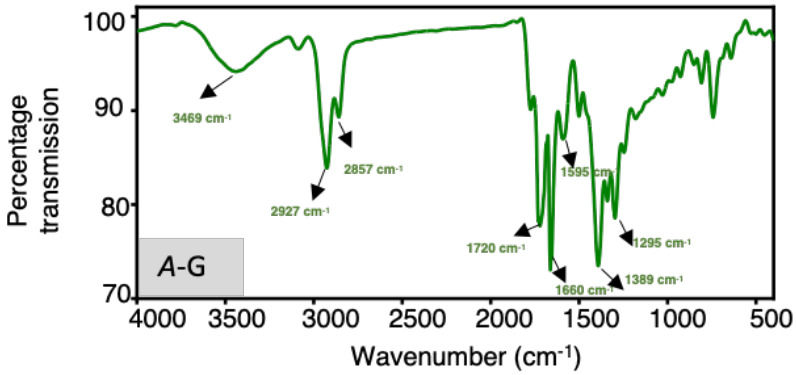

Supplementary Figure 11. FTIR spectrum of ***A*-G** in KBr pellet. The peak near 3600 cm^{-1} is due to the presence of moisture in the KBr pellet. The peaks at 2927 cm^{-1} and 2857 cm^{-1} are due to the alkyl C-H stretching, 1720 cm^{-1} and 1660 cm^{-1} are due to carbonyl stretching (C=O), peak at 1595 cm^{-1} is due to aromatic C=C stretching, 1295 cm^{-1} is due to C-N stretching.

5. The chemical structures of PDI monomers play a critical role in the chiral assembly/nucleation process. The design strategy of chemical structures should be elaborated upon in both the "Introduction" and "Results and Discussion" sections. This includes a detailed discussion on the role of imide-substituents of chiral alkyl chains and bay-substituents of 4-Phenyl-1,2,4-triazolin-3,5-dione, in providing hydrogen bonding or steric effects that influence the interactions between neighboring molecules and, consequently, the nucleation process. To better illustrate this, a model compound may be necessary to compare the proposed effects on regulating the assembly/nucleation process, as well as theoretical calculations.

Ans. We thank the reviewer for this important comment. We have divided the response into three parts, discussing the importance of bay substitution, chiral side chains and theoretical calculations.

(i) Importance of bay substitution:

To validate the importance of bay substitution in the formation of DHS, we used ***S*-PDI** as a model compound because it has the same chiral side chain without any bay substitution. In this case, ***S*-PDI** exists as monomer even after keeping at 25 °C for 14 hours under the conditions where ***S*-G** forms DHS in 48 minutes. When the concentration of ***S*-PDI** increased to 200 μM, under same solvent conditions, its self-assembles over time, as can be seen by the decrease in the absorption spectrum after 3 hours. The morphology analyzed in FE-SEM reveals sharp needles-like morphology but not DHS.

This information is included in the revised manuscript as Supplementary Figure 22, which is given below for your reference.

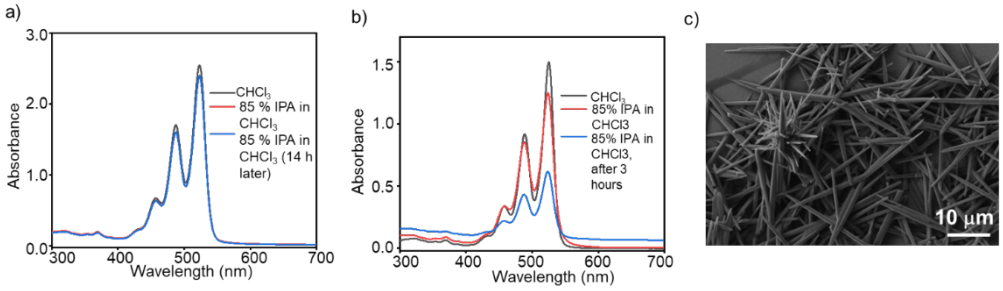

Supplementary Figure 22. (a) Absorbance of a 30 μM solution of ***S*-PDI** in 85 % IPA in $CHCl_3$, (b) Absorbance of a 200 μM solution of ***S*-PDI** in 85 % IPA in $CHCl_3$, (l=1mm) (c) FE-SEM image of 200 μM solution of ***S*-PDI** in 85 % IPA in $CHCl_3$ spin coated on silicon wafer.

(i) Importance of chiral side chain at the imide:

To understand the importance of chiral imide substitution, we have synthesized achiral model compound ***A*-G** using commercially available racemic 2-heptylamine. Similar to ***S*-G**, a 30 μM solution of ***A*-G** in 85 % IPA in $CHCl_3$ shows the temporal evolution of morphology. However, the morphology of self-assembled structures obtained from ***A*-G** are 1D fibers but not DHS. Thus, the presence of a chiral center plays an important role in the formation of DHS.

This information is included in the revised manuscript as Supplementary Figure 21, which is given below for your reference.

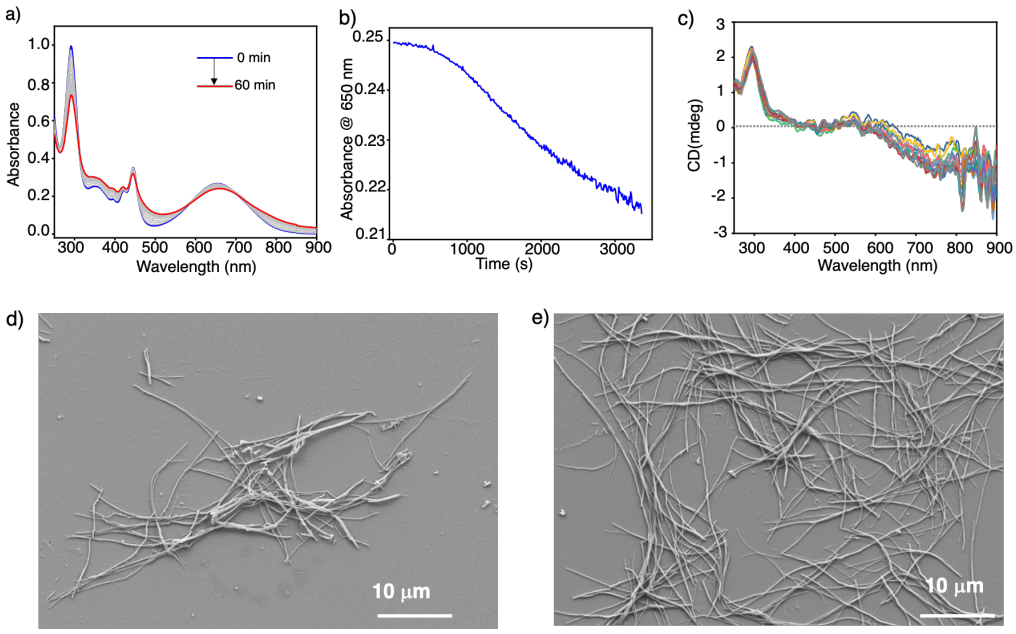

Supplementary Figure 21. (a) Variation in absorption spectra of 30 μM solution of ***A*-G** in 15% $CHCl_3$ in IPA. (b) kinetics of aggregation of ***A*-G** monitored at 650 nm. (c) Time dependant CD spectra show no variation with increasing aggregation. (d) and (e) FE-SEM images of aggregates of ***A*-G** obtained after 3600 seconds.

The following paragraph, which describes the role of bay substitution and chiral side chains experimentally, is included in the revised manuscript at the end of page 6.

"Next, to understand the role of chiral side chains and bay substitution in the formation of DHS, we have investigated the supramolecular polymerization of ***A*-G** and ***S*-PDI**. First to understand the role of chiral side chains, we have synthesized ***A*-G** using commercially available racemic 2-heptylamine. Like ***S*-G** and ***R*-G**, a 30 μM solution ***A*-G** also showed temporal evolution of SPs in 15% $CHCl_3$ in IPA (Supplementary Figure 21a,b). However, the resultant morphology is 1D fibers, not DHS, as evidenced by FE-SEM images (Supplementary Figure 21d,e). As expected, the CD signal of SPs of ***A*-G** is negligible due to achiral nature of the resultant SPs (Supplementary Figure 21c). This indicates that chirality in the side chain is crucial to form DHS. Next, to understand the role of bay substitution, we have investigated the supramolecular polymerization of ***S*-PDI**. We found that a 30 μM solution of ***S*-PDI** in 15% $CHCl_3$ in IPA exists as a monomer even after keeping it at 25 °C for 14 hours (Supplementary Figure 22a). This indicates the weak stacking efficiency of ***S*-PDI** compared to ***S*-G**. At higher concentrations, such as 200 μM, ***S*-PDI** formed self-assembled structures (Supplementary Figure 22b) with needles-like morphology after keeping for 3 hours at 25 °C (Supplementary Figure 22c). Hence, both chirality in the side chain and bay substitution are important for the formation of DHS."

(iii) Theoretical calculations

To understand the role of the bay substitution in improving the stacking efficiency of NIR dyes (***S*-G** and ***R*-G**), we have performed theoretical calculations on both dimers and a stack consisting of 24 monomers in 15% $CHCl_3$ in IPA solvent mixture. The important observations from computational studies are given below.

- Gas-phase quantum mechnical calculations at ωB97XD/6-31G(d) level of theory show that the intermolecular interaction energy between ***S*-G** monomers is approximately 60 kJ/mol higher than that of the ***S*-PDI** monomers, demonstrating that the ***S*-G** dimer is more stable.
- Energy decomposition analysis reveals that the bay-substitution group in the ***S*-G** molecule adds extra stability to the ***S*-G** dimer, primarily by enhancing electrostatic, dispersion, and charge transfer components.
- In comparison with the ***S*-PDI** polymer, the ***S*-G** polymer exhibits superior long-range stacking order and stability.
- The stacking order and stability in the ***S*-G** polymer are mainly attributed to the bay-substituted phenyl ring, which exhibits dynamic characteristics and engages in π-π interactions with neighbouring phenyl rings, as well as CH-π interactions with both neighbouring phenyl rings and hydrocarbon side-chains.

Thus, the bay-substitution in the ***S*-G**, enhances ordering and stabilization of its SPs compared to the ***S*-PDI** while the chiral side chains provide the bias for supramolecular chirality, resulting in the formation of DHS. More details are provided in the Supplementary Note 4 and Supplementary Figures 14, 23-24.

This new data is included in the main text as Figure 4 a, Supplementary Figures 23 and 24, and given below for your reference.

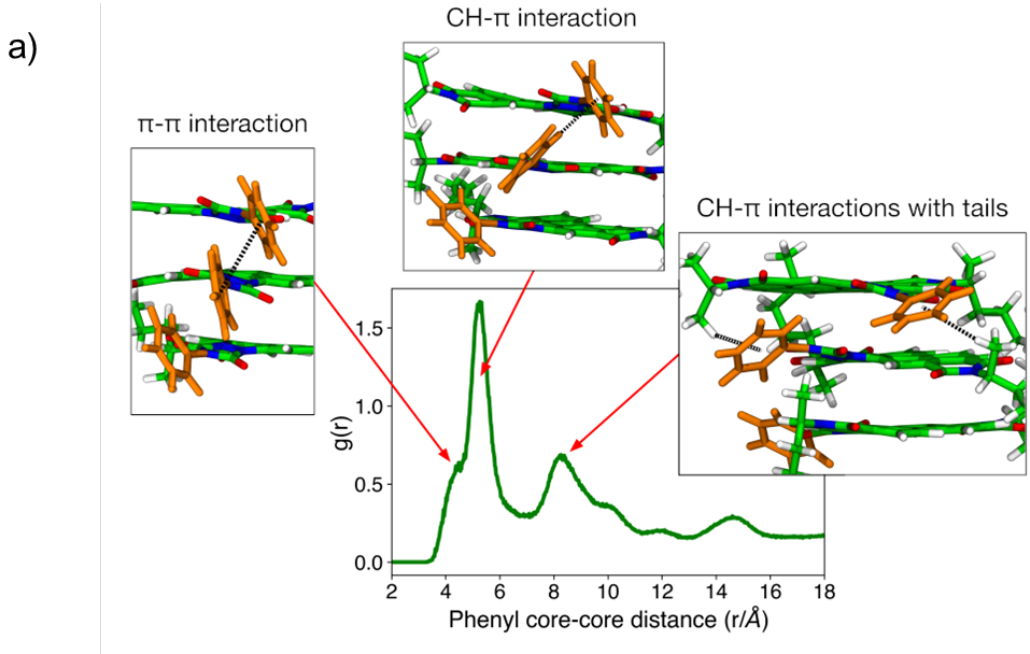

Figure 4. (a) The radial distribution functions (RDF), g(r), between geometric center of phenyl rings in S-G stack. The phenyl rings are observed to engage in three distinct types of interactions within the S-G stack: first, π-π interactions between neighbouring phenyl rings, corresponding to the shoulder at 4.3 Å in the g(r); second, CH-π interactions between adjacent phenyl rings, leading to the peak at 5.2 Å; and third, CH-π interactions between the branched methyl group of one molecule and the phenyl ring of a neighbouring molecule, resulting in the peak at 8.2 Å.

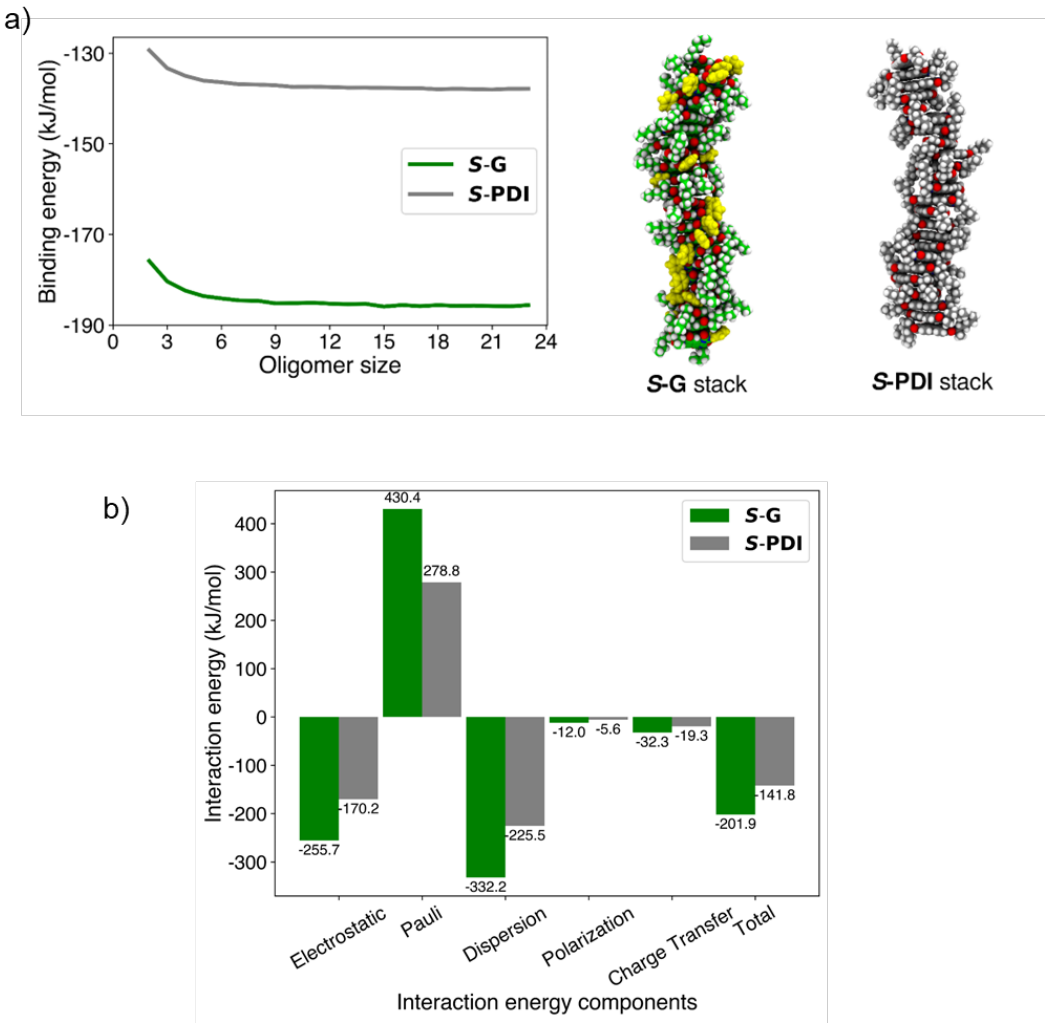

Supplementary Figure 23. (a) Gasphase force field binding energies of ***S*-G** and ***S*-PDI** stacks. The binding energies are calculated using the equation: $(E_n - E_1)/(n-1)$. Results show that the ***S*-G** stack is approximately 50 kJ/mol more stable than the ***S*-PDI** stack. Snapshots of the ***S*-G** and ***S*-PDI** stacks obtained from the equilibrium trajectories are shown on the right side. (b)Energy decomposition analysis of the lowest energy dimers in the gas phase for both ***S*-G** and ***S*-PDI**. This analysis was conducted using the ALMO-EDA framework at the ωB97XD/6-31G(d) level of theory.

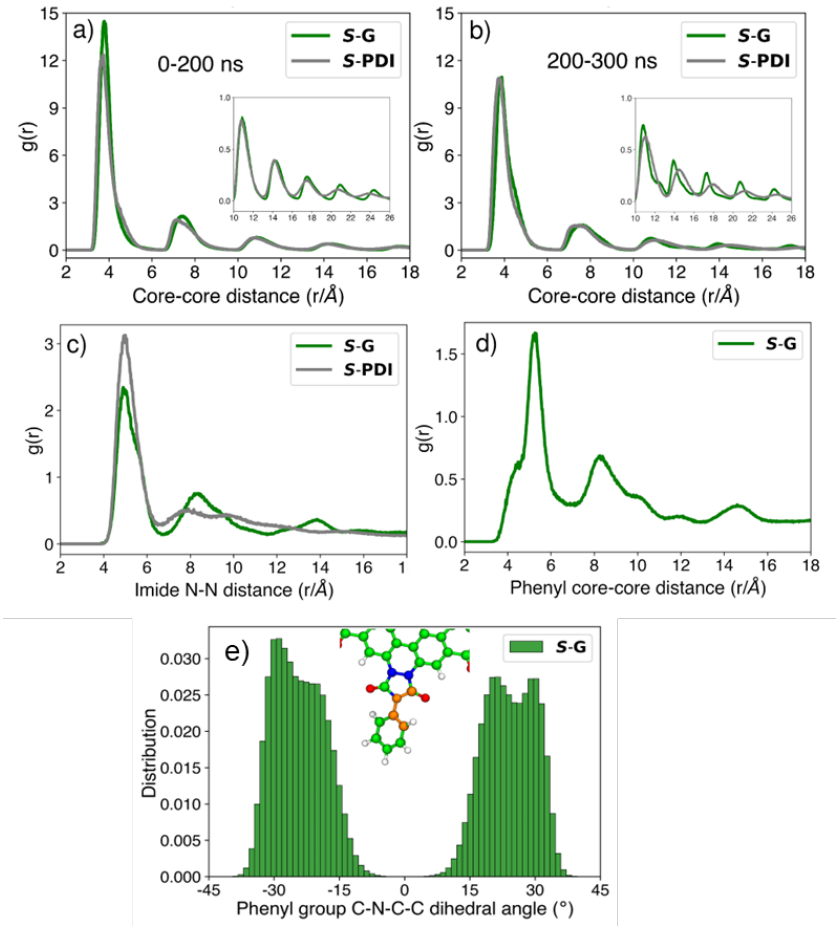

Supplementary Figure 24. The radial distribution function (g(r)) between the geometric centers of the central ring of the aromatic core: (a) derived from the 200 ns MD trajectories, and (b) from an additional 100 ns MD trajectory for both ***S*-G** and ***S*-PDI** stacks. Additionally, (c) shows g(r) between the imide nitrogen atoms and (d) between the geometric centers of the phenyl rings. (e) Distribution of the dihedral angle C-N-C-C (highlighted in orange) associated with the phenyl ring.

The following sentences are included in the introduction part of revised manuscript in page 3 (bottom paragraph).

"Although these NIR dyes have been known for a long time, they have not yet been explored for supramolecular polymerization.[59] The presence of donor groups and a phenyl ring at the bay position not only provides NIR absorption but also significantly enhances their stacking efficiency and order compared to the corresponding perylene diimides (PDIs)[35,60]."

"Under similar conditions, the corresponding PDIs do not self-assemble, and the achiral triimide dye (***A*-G**) forms only 1D fibers, thus highlighting the importance of bay substation and chiral sides in the formation of DHS (Figure 1)."

The following paragraph is included in the revised manuscript in page 7 (second paragraph).

"To further understand the role of the bay substitution in improving the stacking efficiency of NIR dyes (***S*-G** and ***R*-G**), we have performed theoretical calculations on both dimers and a stack consisting of 24 monomers in 15% $CHCl_3$ in IPA solvent mixture. Gas-phase quantum mechanical calculations revealed that the intermolecular interaction energy between ***S*-G** monomers is

approximately 60 kJ/mol higher than that of the ***S*-PDI** monomers, demonstrating that the ***S*-G** dimer is more stable. Energy decomposition analysis indicated that the bay substitution enhances the stability of the ***S*-G** dimer by considerably strengthening the electrostatic, dispersion, and charge transfer interactions. In contrast, the absence of bay-substitution in ***S*-PDI**s results in their self-assembly at relatively higher concentrations, primarily due to their weaker intermolecular interactions compared to those of ***S*-G** molecules. To further investigate the influence of solvent on the stacking propensity and orderliness in the extended fiber, we conducted all-atom classical molecular dynamics simulations on preform stacks in an explicit solvent mixture of 15% $CHCl_3$ in IPA. The presence of strong peaks in the radial distribution function (g(r)) of both systems indicates that both ***S*-G** and ***S*-PDI** stacks are stable in solution.[61] Importantly, the intensity of the first peak is higher for ***S*-G**, suggesting a greater stacking propensity than ***S*-PDI** stacks. The g(r) calculated from the extended trajectory (200-300ns), reveals the emergence of long-range order in the structures of ***S*-G** compared to ***S*-PDI** (Supplementary Figure 24b). This is due to the phenyl rings exhibiting dynamic behaviour, tending to adopt a slanted orientation with an average angle of approximately ±25° relative to the aromatic core (Supplementary Figure 24e). As a result, several additional noncovalent interactions are favoured in the ***S*-G** stack, such as π-π interactions between neighbouring phenyl rings, CH-π interactions between adjacent phenyl rings and CH-π interactions between the branched methyl group of one molecule and the phenyl ring of a neighbouring molecule (Figure 4a). Thus, the bay-substitution in the ***S*-G** enhances the ordering and stabilization of its SPs compared to the ***S*-PDI**, while the chiral side chains provide the bias for supramolecular chirality, resulting in the formation of DHS (See Supplementary Figures 23, 24 and further explanation there)."

6. The manuscript lacks sufficient description and discussion regarding the chiral seed used in the nucleation process. The significance of this component should be addressed more thoroughly.

Ans. We thank the reviewer for this comment. There is no use of chiral seed externally to initiate supramolecular polymerisation. The smaller helical fibres that are formed after the rapid addition of poor solvent (IPA) act as seeds for the secondary nucleation events such as growth on the surface and growth from the surface.

The following sentence are added/modified in page 9, first paragraph of the revised manuscript to elaborate the discussion about seed for secondary nucleation process.

"This indicate that the short 1D helical SPs formed via a primary nucleation event act as seeds for the secondary nucleation events. The increase in the width and length suggests that the remaining monomers in the solution nucleate and elongate on the surface of the short 1D helical SP seeds. This 'growth on the surface' first leads to the formation of a double helix (Figures 3a and 5). The monomers also nucleate from the surface of the seeds to result in branching as evidenced by FE-SEM images (Figures 3a and 5)[64]."

7. Stability in the solid state is crucial for practical applications. The chiroptical sensor demonstration was conducted in solution state. Besides, the supplementary information (SI) only provides the melting temperature of S-G, with no corresponding data for R-G. Additionally, the melting temperature is presented as a number without supporting characterization results such as TGA or other relevant analyses, which should be included

Ans. We thank the reviewer for this comment. To study the thermal stability of ***S*-G**, ***R*-G** and ***A*-G**, we carried out the thermogravimetric analysis (TGA) of all these three compounds. From this data we conclude that the reported compounds are stable until 350 ºC. We also measured the melting point of all three compounds using the Tempo and Mettler FP1 melting point instruments and found that they did not melt until 280 °C.

TGA data is included in the revised manuscript as Supplementary Figure 13, which is shown below for your reference.

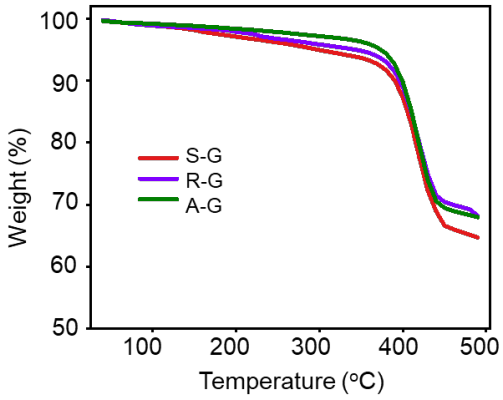

Supplementary Figure 13. TGA profile of ***S*-G** (red curve), ***R*-G** (violet curve) and **A-G** (green curve), measured under N_2 gas flow of 100 mL min^{-1} and heating rate of 10 °C min^{-1}.

The following sentence regrading TGA is included in the revised manuscript page 4, bottom paragraph.

"Thermogravimetric analysis reveals that all three triimide dyes are thermally stable up to 350 °C (Supplementary Figure 13)."

8. Zoomed-in images of the helical fiber branches should be included to demonstrate the homochirality in relation to the superhelix center within the resulting superstructures

Ans. We thank the reviewer for this comment. To assess the helicity of the self-assembled fibers, microscopic techniques such as FE-SEM and AFM were used. As can be seen by the AFM and FE-SEM images, the central superhelix and the branching of the end fibers all follow the same chirality. DHS formed from ***S*-G** have a right-handed helical organization and the DHS of ***R*-G** have a left-handed helical organization.

This new data is added to the revised manuscript as Supplementary Figures 19 and 20.

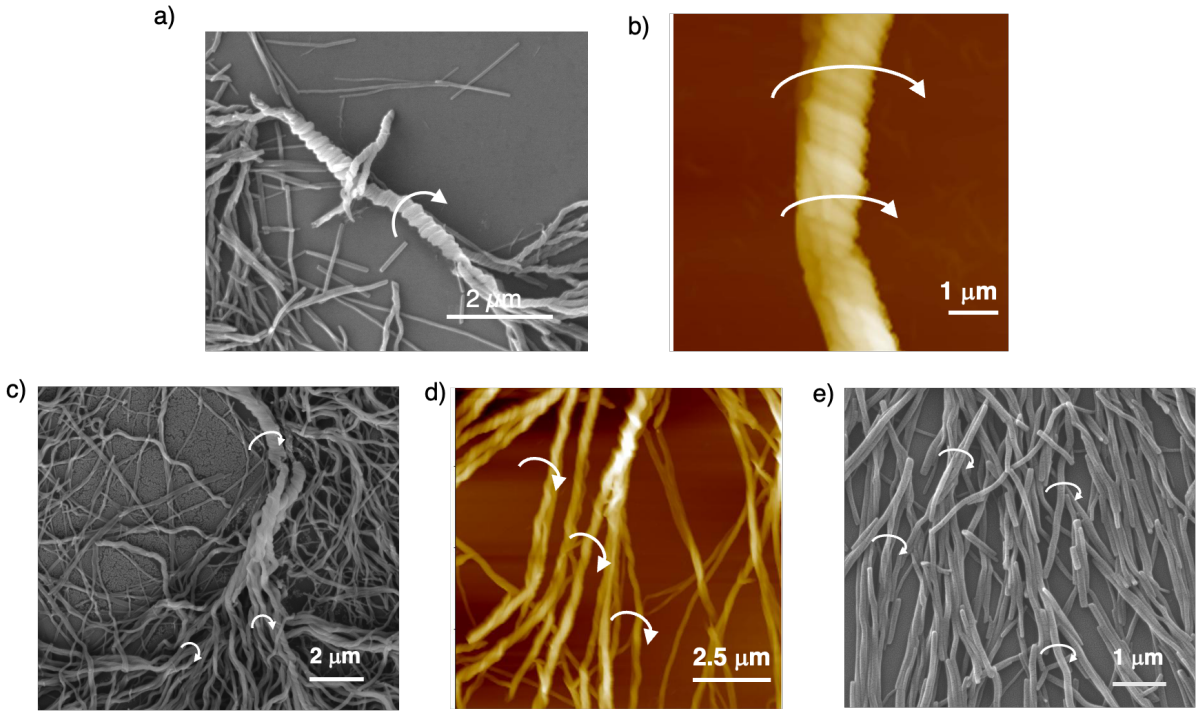

Supplementary Figure 19. FE-SEM and AFM images of DHS of ***S*-G** showing righthanded homochirality. (a) FE-SEM and (b) AFM images of superhelix of DHS of ***S*-G**. (c) FE-SEM image of branches in DHS showing righthanded helicity. (d) AFM and (e) FE-SEM images of thin helical fibers of DHS. These samples are prepared by spin-coating a 30 μM solution of ***S*-G** in 15% $CHCl_3$ in IPA on a silicon wafer.

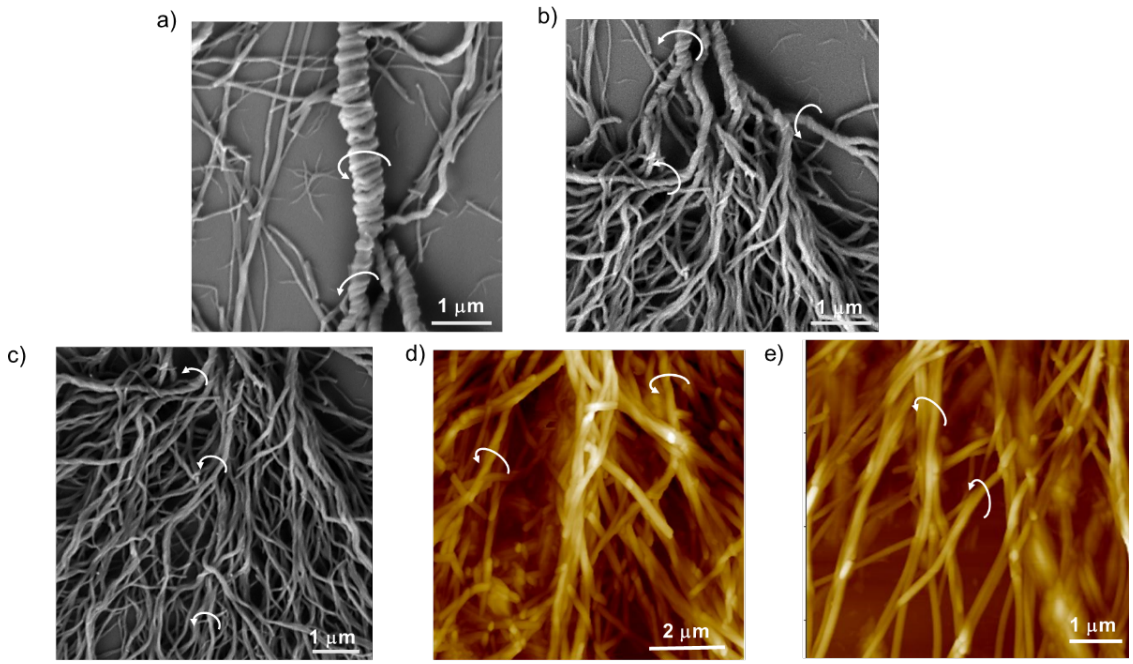

Supplementary Figure 20. FE-SEM images and AFM images of DHS of ***R*-G** showing lefthanded chirality and homochirality. (a) FE-SEM image of superhelix of DHS of ***R*-G**. (b) FE-SEM image of branches of DHS of ***R*-G**. (c) FE-SEM image of branches and thin fibers showing homochirality in DHS of ***R*-G**. (d) and (e) AFM images of thin helical fibers of DHS. These samples are prepared by spin-coating a 30 μM solution of ***R*-G** in 15% $CHCl_3$ in IPA on a silicon wafer.

The following sentences are included in the revised manuscript on page 6, top paragraph.

"Further analysis of FE-SEM and atomic force microscopy (AFM) images revealed that the central superhelix and branched thin helical fibers formed from ***S*-G** have a right-handed helical orientation (Supplementary Figure 19). Similarly, FE-SEM and AFM images revealed the left-handed helical orientation for DHS formed from of ***R*-G** (Supplementary Figure 20). These observations not only confirm the opposite helicity of DHS formed from ***S*-G** and ***R*-G** but also their homochiral nature."

9. There are a few typographical errors. On page 3, line 70, the phrase "...a remarkable advancement in his field for the synthesis" should be corrected to "...in this field..." Additionally, there should be a space between the number and "V" (voltage).

Ans. We thank the reviewer for pointing out this mistake, these mistakes are now been rectified in the main manuscript.

NCOMMS-24-46135A

Point-to-Point responses to the reviewer's comments

We thank all the reviewers for the recommendation of our manuscript for publication in *Nature Communications*.

The responses to the reviewer's comments are given below.

Reviewer-1

All of my comments and concerns have been well and thoroughly addressed in this new version. I congratulate the authors on this beautiful work and thank them for investing the time to substantially improve the previous version! I would like to recommend to accept this paper as is.

Ans. We thank the reviewer for appreciating our work and recommending it for publication.

Reviewer-2

The manuscript has been properly revised and can be accepted for publication.

Ans. We thank the reviewer for recommending our manuscript for publication.

Reviewer -3

The discovery is intriguing. Following the initial review process, the authors have conducted additional experiments, including the synthesis of achiral model compounds and relevant calculations. Overall, the quality of the paper has improved by addressing the feedback from the three reviewers. However, some formatting issues still need to be addressed, such as maintaining consistency in time units (e.g., 'sec' vs. 'seconds'), correcting grammatical errors, and ensuring uniformity in the range and height of the ^1H NMR spectra.

Ans. We thank the reviewer for appreciating our work and the additional experiments performed during revision. Throughout the manuscript, we have used only 'sec.' and corrected grammatical errors. We have also maintained the uniformity of ^{1}H-NMR data, such as range and height, in the revised Supplementary Information (Please see Supplementary Figures 2, 6 and 10).

.

Reviewer #3 attachment:

In this work, the authors reported the formation of dendritic homochiral superstructures through the secondary nucleation of perylene diimide derivatives. The resulting superstructures consist of a superhelix center with helical fiber branches, covering an area of approximately 0.4 mm^2. While the optical images are visually appealing, the experimental details and discussions are insufficient. Consequently, this manuscript appears to report a phenomenon rather than providing scientific insights that would be valuable for peer researchers. Therefore, the manuscript is not suitable for publication in *Nature Communications* at this stage. The following issues need to be addressed:

1. The characterization of the chemical structures of S/R-G requires further enhancement. In the 1H NMR spectra, the corresponding peaks in S/R-G show shifts of approximately 0.3 ppm (e.g., 9.30 ppm vs 9.03 ppm). This raises concerns about whether the 1H NMR is properly calibrated; if it is, an explanation for these shifts should be provided. The MALDI-TOF spectra should also include a zoomed-in view to clearly display the isotope patterns of the respective peaks. Additionally, the FTIR spectra of S-G and R-G differ significantly, with R-G exhibiting more intense peaks around 3500 cm^{-1}, which are unexpected and warrant explanation. Furthermore, S-G displays more pronounced C-O peaks around 2400 cm^{-1} compared to R-G, potentially indicating the presence of CO_2. This suggests that the quality of the FTIR data should be improved."

2. The chemical structures of PDI monomers play a critical role in the chiral assembly/nucleation process. The design strategy of chemical structures should be elaborated upon in both the “Introduction” and “Results and Discussion” sections. This includes a detailed discussion on the role of imide-substituents of chiral alkyl chains and bay-substituents of 4-Phenyl-1,2,4-triazolin-3,5-dione, in providing hydrogen bonding or steric effects that influence the interactions between neighboring molecules and, consequently, the nucleation process. To better illustrate this, a model compound may be necessary to compare the proposed effects on regulating the assembly/nucleation process, as well as theoretical calculations.

3. The manuscript lacks sufficient description and discussion regarding the chiral seed used in the nucleation process. The significance of this component should be addressed more thoroughly.

4. Stability in the solid state is crucial for practical applications. The chiroptical sensor demonstration was conducted in solution state. Besides, the supplementary information (SI) only provides the melting temperature of S-G, with no corresponding data for R-G. Additionally, the melting temperature is presented as a number without supporting characterization results such as TGA or other relevant analyses, which should be included.

5. Zoomed-in images of the helical fiber branches should be included to demonstrate the homochirality in relation to the superhelix center within the resulting superstructures

6. There are a few typographical errors. On page 3, line 70, the phrase “…a remarkable advancement in his field for the synthesis” should be corrected to “…in this field…” Additionally, there should be a space between the number and “V” (voltage).